DOI: 10.1002/chem.200801405

Reaching Optimal Light-Induced Intramolecular Spin Alignment within Photomagnetic Molecular Device Prototypes

Ilaria Ciofini,*[a] Carlo Adamo,[a] Yoshio Teki,[b] Fabien Tuyèras,[c] and Philippe P. Lainé*[c]

Abstract: Ground-state (GS) and excited-state (ES) properties of novel photomagnetic molecular devices (PMMDs) are investigated by means of density functional theory. These organic PMMDs undergo a ferromagnetic alignment of their intramolecular spins in the lowest ES. They are comprised of: 1) an anthracene unit (An) as both the photosensitizer (P) and a transient spin carrier (SC) in the triplet ES (^{3}An*); 2) imino-nitroxyl (IN) or oxoverdazyl (OV) stable radical(s) as the dangling SC(s); and 3) bridge(s) (B) connecting peripheral SC(s) to the An core at positions 9 and 10. Improving the efficiency of the PMMDs involves strengthening the ES intramolecular exchange coupling (J_{ES}) between transient and persistent SCs, hence the choice of 2-pyrimidinyl (pm) as B elements to replace the original *p*-phenylene (ph). Dissymmetry of the pm connectors leads to [SC-B-P-B-SC] regio-isomers *int*. and *ext.*, depending on whether the pyrimidinic nitrogen atoms point towards the An core or the peripheral SCs, respectively. For the *int*. regio-isomers we show that the photo-induced spin alignment is significantly improved because the J_{ES}/k_B value is increased by a factor of more than two compared with the ph-based analogue ($J_{ES}/k_B > +400$ K). Most importantly, we show that the optimal J_{ES}/k_B value ($\approx +600$ K) could be reached in the event of an unexpected saddle-shaped structural distortion of the lowest ES. Accounting for this intriguing behavior requires dissection of the combined effects of 1) borderline intramolecular steric hindrance about key An–pm linkages, which translates into the flatness of the potential energy surface; 2) spin density disruption due to the presence of radicals; and 3) possibly intervening photochemistry, with An acting as a light-triggered electron donor while pm, IN, and OV behave as electron acceptors. Finally, potentialities attached to the [(SC)-pm-An-pm]$_{int}$ pattern are disclosed.

Keywords: density functional calculations · functional emergences · magnetic properties · molecular spintronics · radicals

Introduction

There is no better choice than light for interacting with molecules. Light can be used 1) as a probe to address molecular entities; 2) as a trigger to manipulate molecular properties;

[a] Dr. I. Ciofini, Prof. Dr. C. Adamo
Laboratoire d'Électrochimie et
Chimie Analytique (CNRS UMR-7575)
École Nationale Supérieure de Chimie de Paris
11, rue Pierre et Marie Curie, 75231 Paris Cedex 05 (France)
Fax: (+33) 144-276-750
E-mail: ilaria-ciofini@enscp.fr

[b] Prof. Dr. Y. Teki
Department of Material Science
Graduate School of Science
Osaka City University
3-3-138 Sugimoto, Sumiyoshi-ku, Osaka 558–8585 (Japan)

[c] Dr. F. Tuyèras, Dr. P. P. Lainé
Laboratoire de Chimie et Biochimie Pharmacologiques et
Toxicologiques (CNRS UMR-8601)
Université Paris Descartes, Faculté de Médecine
45, rue des Saints Pères, 75270 Paris Cedex 06 (France)
Fax: (+33) 142-868-387
E-mail: philippe.laine@univ-paris5.fr

Supporting information for this article is available on the WWW under http://dx.doi.org/10.1002/chem.200801405. It includes: Computed geometrical parameters for **Td*n***, **Dd*n***, **Td*n**** and **Dd*n**** ($n = 5$–8) and for **HTd71** and **HTd72** in both the GS and the ES (three tables); Computed highest SOMO for **Dd5***, **Td5*** and **Ref5*** (in both axially distorted and saddle-shaped distorted conformations); Analysis of bond-length alternation patterns in **Dd5*** (vs. **Dd5**) and **Td5*** (vs. **Td5**); Optimized structures of **HTd71***, **HTd72***, **Td3bis***, **Td4bis*** and for **Ref5** and **Ref6** in both their mono-reduced and mono-oxidized states; Calculated spin-density patterns for **Dd6** and **Td6** (with contour values of 5×10^{-4} and 5×10^{-5} a.u.) and for **Td3bis*** and **Td4bis***; One figure showing pictorially the minor contribution of resonance forms attached to ICTs within **Ref5*** in the lowest ES.

 © 2008 Wiley-VCH Verlag GmbH & Co. KGaA, Weinheim

3) as a quantum of energy to fuel the activity of molecular machinery; and/or 4) as a quantum of information (input) to be handled at the molecular level.[1] Photochemical molecular devices (PMDs),[2] are typically light-driven molecules devised to act at their level for carrying out a specific task. They merit being referred to as supermolecules.[3] The paradigm of PMDs comes from a combination of original paradigms of supramolecular chemistry[4] and molecular (inorganic) photochemistry, which were adapted for the intramolecular medium and in particular for properties and functions relying on an electronic basis.[1b] These functional supermolecules are often quite imposing in size as a result of their multicomponent nature. They are made up of weakly interacting components at the electronic level and are justly referred to as weakly coupled systems, the features of which are accurately accounted for by a localized description. These supermolecules must be distinguished from large molecules, which are conversely described within a delocalized framework, featuring made-in-one-piece electronic behaviors.[3,5,6]

As part of our continuing research program to control and manipulate intramolecular electronic and magnetic couplings, we are interested in closely coupled (compact) multicomponent systems.[7–11] Our efforts are essentially directed towards the related fields of artificial photosynthesis and molecular electronics[7,12,13] (including molecular spintronics[10c,14]). Inter alia, our work is aimed at incorporating "strong and tunable intercomponent electronic and/or magnetic couplings" as full functional ingredients[10,11,14–16] into a new type of PMDs, while retaining the hallmarks of supermolecules.[2,3,5] "By skating on the edge of the paradigm"[17] of PMDs, we presently investigate the borderline case of closely coupled and affiliated light-interacting systems, which may dramatically change their behavior (e.g., from that of supramolecular composite species, supermolecules, to that of made-in-one-piece large molecules)[7,9] upon slight alteration of the connection scheme of their functional components. As well as searching for new molecular photoswitching principles,[9] the present study is aimed at both 1) improving the photomagnetic functioning of a new type of PMDs, namely photomagnetic molecular devices (PMMDs),[14] and 2) gaining some basic knowledge relative to the boundaries of multifunctional integration at the molecular level.

PMMDs are the PMDs that were recently adapted to support additional magnetic properties to perform operations of potential interest in the nascent field of molecular spintronics.[10c,14,18] These PMMDs are viewed as advanced molecular-electronics devices, intended to rely on the spin of the electron rather than on its charge to handle information at the molecular level.[14] In this context, PMMD prototypes[14] were recently designed by one of us[10] (Figure 1) to undergo a photoinduced alignment of their intramolecular spins. These organic entities are systems of choice to study closely coupled molecular assemblies, because improving their magnetic properties involves optimizing (here increasing) intercomponent electronic couplings. Indeed, an intrinsic feature of these PMMDs is the fairly strong intercomponent coupling they require for efficient mediation of (super)exchange magnetic interaction (J). For this specific reason, these molecular devices are potentially fully π-conjugated systems. Of importance for the present work is the recognized sturdiness[14] of the magnetic properties in the sense that, contrary to usual electronic features, magnetically active components of molecular assemblies can stand (very) large electronic coupling and still fit in a localized description reminiscent of that used for supermolecules in the field of supramolecular photochemistry.[14] Magnetism is, therefore, a means to trace the behavior of systems showing increasing intercomponent electronic coupling up to the disappearance of the original electronic features of individual components. It is also well established, however, that the presence of a permanent source of paramagnetism (such as stable radicals) within a PMD assembly contributes to a slackening of some of the conventional selection rules[19] and is therefore likely to disrupt its photochemical functioning, as we will show here.

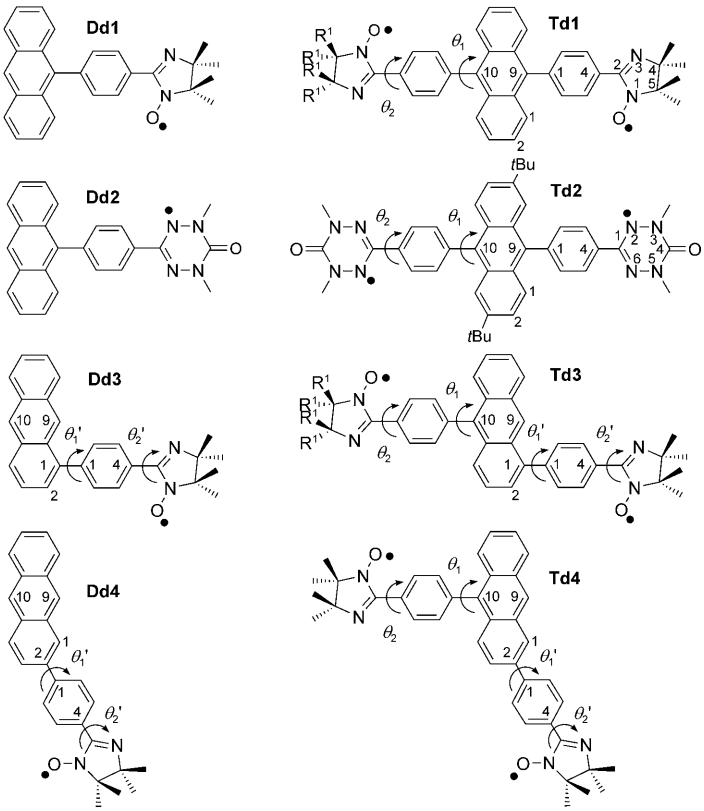

Figure 1. Schematic drawing together with labeling and numbering schemes of PMMDs (**Dd*n***, **Td*n***) already investigated experimentally ($n=$ **1**, **2**)[10] and theoretically ($n=$**1**–**4**).[14]

The multicomponent (polyad) systems herein considered are made up of the following functional elements:[14] 1) one photosensitizer unit (P), namely anthracene (An), capable of photo-switching from its diamagnetic (closed-shell) ground state (GS) to its paramagnetic (e.g., open-shell triplet radical) excited state (ES); 2) peripheral spin carriers

 © 2008 Wiley-VCH Verlag GmbH & Co. KGaA, Weinheim

(SCs), which are typically stable organic radicals like iminonitroxyl (IN)[20] and oxoverdazyl (OV); and 3) bridging elements (B), which are connectors mediating the exchange interaction between the central P and the dangling SCs. Basically, the working principle of such PMMDs is the following (Scheme 1). In the initial ground state, the peripheral SCs

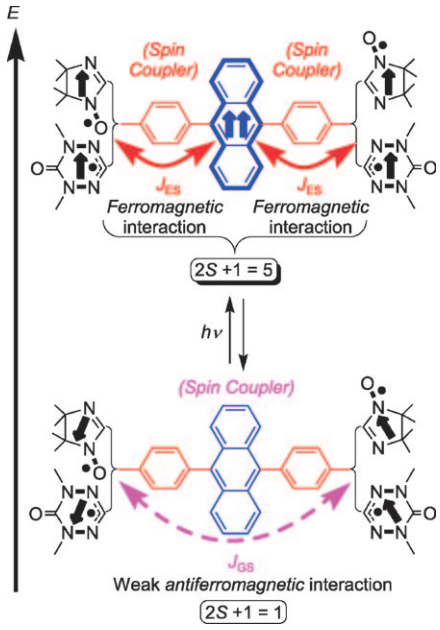

Scheme 1. Working principle of the PMMDs studied.[10g–j14]

are loosely antiferromagnetically coupled ($J_{GS} \leq 0$) through the diamagnetic [B-P-B] assembly as the spin coupler. Upon light excitation, P is promoted into its paramagnetic lowest excited state (^{3}P*), thus transiently behaving as a full SC in the same capacity as other persistent ones.[14] As a result of enhanced and selective intersystem crossing, P* becomes ferromagnetically coupled ($J_{ES} > 0$) with the remote SCs through the spin-polarized B subdivisions (the spin couplers in the ES). The transient intramolecular spin alignment thus obtained translates into a change of the overall molecular spin state from $S=0$ in the GS to $S=2$ in the ES. It is noteworthy that P is not only a chromophore or SC in the excited state (P* = SC), but also functions as the effective nexus for the intramolecular spin alignment.

We have recently perfected a computational approach to assess quantitatively the exchange coupling constant, J, in the excited state (J_{ES}),[14] of well-documented diradical species (Figure 1), for which such a quantity is not straightforwardly accessible by experimental means. The same theoretical approach is applied here to predict the photomagnetic behavior of new mono- and diradical species. On this theoretical basis, we show that it is now possible to rationally improve the efficiency of these prototypical PMMDs by adjusting their functional elements.

We have also showed previously[14] that the best connection scheme for the functional elements is when the linkers B are connected at positions 9 and 10 of anthracene, in which the larger atomic spin populations (ASP) lie in the triplet excited state. The superexchange magnetic coupling between the central transient magnetic "supersite"[14] (^{3}An*) and remote persistent magnetic sites is essentially governed by the θ_1 tilt angle ($\theta_1 = 65°$; Figure 1),[14] as the θ_2 twist angle remains optimum for the exchange interaction when connectors (B) are phenylenes (that is, roughly 0°) regardless of the nature (IN/OV) of the terminal SC. The main obstacle with respect to key overall π-conjugation thus originates from steric hindrance between the hydrogen atoms of the phenyl spacers and the *peri* hydrogen atoms of the An lateral rings, hence the determining role promised[14] for the bridging elements (B).

Herein we report how proper substitution of intervening phenyls (ph; Figure 1) for the less sterically burdened,[21] anisotropic and potentially redox-active 2-pyrimidinyl (pm) rings allows the steric congestion about the P-B linkages to be completely overcome. Actually, this molecular design led to two types of photomagnetic improvements, respectively stemming from: 1) the anticipated increase of J_{ES} related to the programmed decrease of θ_1 within the supermolecule; and 2) a further increase of J_{ES} related to an unexpected light-induced emerging behavior typical of an electronically made-in-one-piece large molecule. The extreme sequence sensitivity of the functional connection schemes including upon the vector nature of the pm B element (regio-isomerism) is illustrated throughout the study of affiliated[22] dyads (**Dd*n***; $n = 5$–8) and triads (**Td*n***; $n = 5$–8) shown in Figure 2. The improvement of this type of PMMDs is such that they are anticipated to be workable at room temperature ($J_{ES}/k_B > +298$ K; k_B is the Boltzman constant). We also show that the combination of borderline steric hindrance, small charge transfers, and radical-induced spin-density perturbation are the determining intramolecular factors for the emerging behavior, which is embodied in a peculiar saddle-shaped structural distortion of the lowest excited states and attached electronic, magnetic, and intriguing photophysical features.

Computational Methods

All calculations were performed using the Gaussian 03 package.[23] The hybrid PBE0 exchange-correlation functional,[24] casting 25% of Hartree–Fock exchange in the parent generalized gradient approximation (GGA) functional (i.e., PBE),[25] was used throughout, within unrestricted formalism, for calculations of structural, electronic, and magnetic properties.

Unless otherwise specified, structural optimizations and subsequent frequency calculations were performed using the Dunning–Hay double-zeta-valence basis set,[26] hereafter referred to as the LANL2 basis.

Larger basis sets were used to compute magnetic properties, that is, the isotropic-exchange-coupling constant (J). For such calculations, a Pople double-zeta-split valence basis (6-31G)[27] was used for all atoms belonging to the central (di)pyrimidine-anthracene unit, whereas all other non-hydrogen atoms were described by the same basis enhanced by one d polarization function and a diffuse function as well (6-31+G(d)).[27] This ensemble of basis sets will be referred to as Pople$_{mix}$ in the following.

 © 2008 Wiley-VCH Verlag GmbH & Co. KGaA, Weinheim

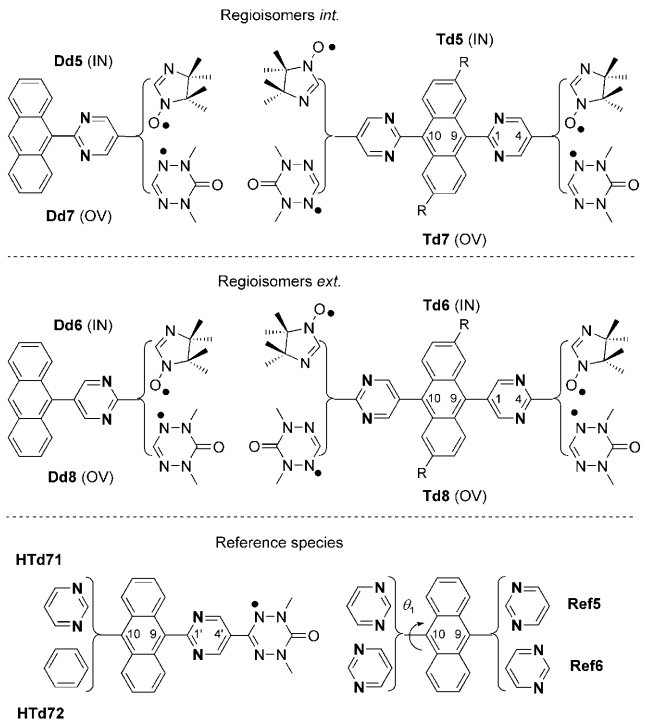

Figure 2. Schematic drawing together with labeling and numbering schemes of the main PMMDs and reference species theoretically studied in this work. R = H and *t*Bu for IN-based and OV-based triads (**Td*n***), respectively. For nomenclature (*int./ext.*), see text.

The magnetic-exchange interaction between the radical units was interpreted by using the Heisenberg–Dirac–Van Vleck (HDVV) spin Hamiltonian, given in Equation (1).[28–30]

$$H_{HD} = -2 \sum_{i,j} J_{ij} \vec{S}_i \vec{S}_j \quad (1)$$

Using this notation, negative J values correspond to an antiferromagnetic interaction, whereas positive ones are related to a ferromagnetic interaction. To compute the J values, the broken-symmetry (BS) approach was applied.[31–34] In particular, J was computed as given in Equation (2), in which $\langle S^2 \rangle_{HS}$ and $\langle S^2 \rangle_{BS}$ are the expectation value of S^2 computed for the high spin (HS) and broken symmetry states, respectively.

$$J_{ij} = -\frac{(E_{HS} - E_{BS})}{\langle S^2 \rangle_{HS} - \langle S^2 \rangle_{BS}} \quad (2)$$

The total energy convergence for both HS and BS states was set at 10^{-8} Hartrees. J values, reported in the Tables as J/k_B, are expressed in K units to facilitate comparison with available experimental data.

In the following, all excited states will be suffixed with *. Finally, when atomic spin populations (ASP) or charges are discussed, we always refer to Mulliken analyses.

Results and Discussion

The relevance of the present theoretical approach, including the use of the HDVV formalism, which requires that magnetic features of the molecules fit a localized description,[35] has been checked recently against available experimental data.[14] Thus, [P*-(B)-SC] photoexcited two-component systems (dyads, **Dd*n****) are suitable model molecules for both the quantitative theoretical calculation[14] and the qualitative experimental evaluation[10] of intramolecular exchange coupling constants in the excited state (J_{ES}; Scheme 1). On the other hand, [SC-(B)-P-(B)-SC] three-component systems (triads, **Td*n***) are good model molecules for assessing the exchange-coupling interaction in the ground state (J_{GS}) between the remote SCs through the diamagnetic -(B)-P-(B)- spin coupler (Scheme 1). For the sake of clarity and simplification, the terminology of "polyads" adopted here only takes into account the number of magnetic sites whether permanent (SC) or potential (P gives transient $^3P^* = SC$) as active functional components (Scheme 1). It remains, nonetheless, that the role of intervening B connector units is critical, as they mediate the polarization patterns of influential spin providers (SCs and P*). Here theoretical tools are essentially used to assess the functional relevance of B elements, and we show that this is, indeed, worthwhile.

Insights into structural features of ground and lowest THEXI states: Intramolecular geometry (conformation) does play a pivotal role in closely coupled and potentially fully π-conjugated systems.[8a,b,9,14,36] Relaxed geometries of both the ground and the lowest thermally equilibrated excited (THEXI) states have been, therefore, carefully computed. Regarding the ground states, even if spin-carriers are antiferromagnetically coupled within triads, geometry optimizations have been carried out on the slightly higher lying pure triplet states ($S = 1$). Indeed, we have shown[14] that the optimized structures of broken symmetry (BS) states ($m_s = 0$) and corresponding triplet states ($S = 1$) are virtually identical, owing to the small coupling of the radicals in the ground state. Regarding the lowest THEXI states, for which the magnetic sites are ferromagnetically coupled,[10,14] they were calculated as quartets (Qr; $S = 3/2$) and quintets (Qn; $S = 2$) for dyads and triads, respectively.

The lone pairs of the heterocyclic nitrogen atoms are sterically less demanding than hydrogen atoms, hence the idea of replacing the phenyl (ph) connectors (Figure 1) with 2-pyrimidinyl (pm) rings (Figure 2) to reduce the steric encumbrance[21] between the photosensitizer (P) and intervening B units, thereby decreasing the θ_1 tilt angle. The point is that allowing better π-conjugation is likely to enhance the magnetic exchange interactions in both the ground and the excited states. The favorable configuration to alleviate steric congestion about the P-(θ_1)-B linkage is thus when the nitrogen atoms of pm point towards the anthracene *internal* core (**Dd5**, **Td5**, **Dd7**, and **Td7**; Figure 2). In the following, we refer to these species as regio-isomers *int*. Other isomers with the pyrimidinic nitrogen atoms pointing towards the *external* dangling radical(s) (**Dd6**, **Td6**, **Dd8**, and **Td8**; Figure 2) are referred to as regio-isomers *ext.*, and were also investigated for the sake of rationalization. The computed structural parameters of the relaxed geometries are gathered in Tables S I and S II in the Supporting Information. Only the most salient features are collected in Tables 1 and 2. Even if the main difference between various PMMDs con-

 © 2008 Wiley-VCH Verlag GmbH & Co. KGaA, Weinheim

Table 1. Selected structural parameters computed for imino-nitroxide (IN) derivatives in the ground (**Td5**, **Dd5**, **Td6**, **Dd6**) and in the excited states (**Td5***, **Dd5***, **Td6***, **Dd6***). Distances in Å, angles in degrees. For labeling system refer to Figures 1–3.

	Regio-isomers *int.*				Regio-isomers *ext.*			
	Dd5 $S=1/2$	**Dd5*** $S=3/2$	**Td5** $S=1$	**Td5*** $S=2$	**Dd6** $S=1/2$	**Dd6*** $S=3/2$	**Td6** $S=1$	**Td6*** $S=2$
dC9^{An}–C1^{Pm}	1.484	1.442	1.487	1.439	1.485	1.469	1.485	1.472
dC4^{Pm}–C2^{IN}	1.464	1.451	1.465	1.453	1.480	1.478	1.481	1.479
θ_1	51.7	(11.6)	59.3	(0.4)	70.2	56.4	72.3	59.1
θ_2	2.9	0.0	2.6	1.2	62.4	58.1	63.3	59.7
$\varphi=180-\varphi'$	(0)	75.4	(0)	81.5	(0)	(0)	(0)	(0)
α_1/α_2	(0)	26.8	(0)	27.5	(0)	(0)	(0)	(0)
dC9^{An}–C10^{An}/r	2.834	2.858	2.849	2.831	2.833	2.856	2.853	2.883

Table 2. Selected structural parameters computed for oxoverdazyl (OV) based dyads (**Dd7**, **Dd8**) and triads (**Td7**, **Td8**) in both the ground and the excited (*) states. Distances in Å, angles in degrees. For labeling system refer to Figures 1–3.

	Regio-isomers *int.*				Regio-isomers *ext.*			
	Dd7 $S=1/2$	**Dd7*** $S=3/2$	**Td7** $S=1$	**Td7*** $S=2$	**Dd8** $S=1/2$	**Dd8*** $S=3/2$	**Td8** $S=1$	**Td8*** $S=2$
dC9^{An}–C1^{Pm}	1.485	1.438	1.487	1.437	1.484	1.463	1.485	1.465
dC4^{Pm}–C1^{OV}	1.470	1.455	1.470	1.458	1.484	1.480	1.484	1.480
θ_1	53.4	(1.6)	60.7	(2.4)	70.5	52.9	73.5	54.3
θ_2	0.3	0.1	0.6	0.7	39.8	0.4	40.3	11.5
$\varphi=180-\varphi'$	(0)	77.8	(0)	80.5	(0)	(0)	(0)	(0)
α_1/α_2	(0)	28.6	(0)	28.0	(0)	(0)	(0)	(0)
dC9^{An}–C10^{An}/r	2.834	2.854	2.847	2.834	2.835	2.861	2.862	2.894

cerns the bridging unit B including regio-isomers *int.* and *ext.*, the results are presented as a function of the nature of the persistent SCs, namely imino-nitroxyl (IN; Table 1) and oxoverdazyl (OV; Table 2). The structural parameters used to describe the relaxed ground states and lowest thermally-equilibrated excited states are given in Figure 3.

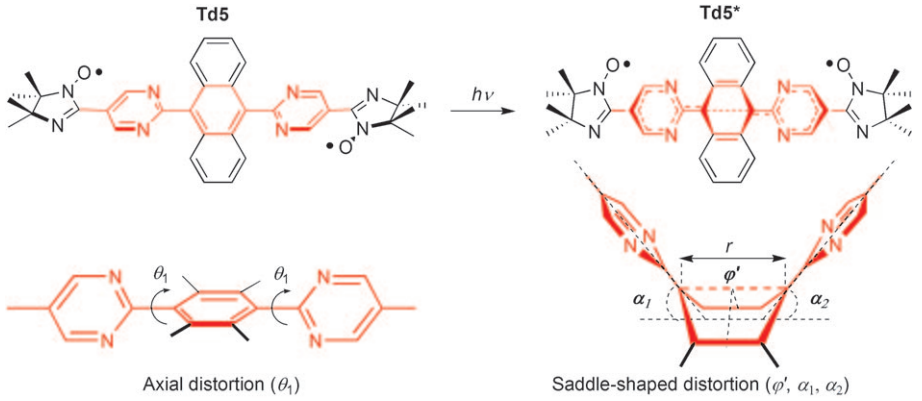

Figure 3. Structural parameters used to describe axially distorted states (whether ground or excited) together with parameters specifically used for saddle-shaped excited states. Illustrative case of **Td5** (top and side views).

Insights into structural features of the ground states: All polyads, including [B-(θ_1)-P-(θ_1)-B] references species (**Ref5** and **Ref6**; Table 3), show virtually the same axially distorted geometry in the ground state as that adopted by ph-based PMMDs (Figure 1).[14] This conformation is characterized by non-zero values of the θ_1 tilt angle and also, to a lesser extent, by the θ_2 twist angle.

The ground-state structural features of IN-based PMMDs (that is, **Dd5**, **Dd6**, **Td5**, and **Td6**) were analyzed first. The

Table 3. Selected structural parameters computed for reference 9,10-di-pyrimidinyl-anthracene regio-isomers *int.* and *ext.* in both the ground and the excited (*) states. Distances in Å, angles in degrees. For labeling system refer to Figures 2 and 3.

	[pm-An-pm]$_{int}$ (**Ref5**), $S=0$	**[pm-An-pm]$_{int}$*** [a] (**Ref5***), $S=1$	**[pm-An-pm]$_{ext}$** (**Ref6**), $S=0$	**[pm-An-pm]$_{ext}$*** (**Ref6***), $S=1$
dC9^{An}–C1^{Pm}	1.489	1.446 (*sd.*)/1.473 (*ax.*)	1.486	1.476
θ_1	61.8	0.8 (*sd.*)/46.5 (*ax.*)	75.1	62.5
$\varphi=180-\varphi'$	(0)	33.3	(0)	(0)
α_1/α_2	(0)	29.2	(0)	(0)
dC9^{An}–C10^{An}/r	2.848	2.825	2.855	2.880

[a] Two different conformations (axially and saddle-shaped distorted denoted *ax.* and *sd.*, respectively) can be computed, but only one (*sd.*) corresponds to a minimum (see text).

 © 2008 Wiley-VCH Verlag GmbH & Co. KGaA, Weinheim

most salient computed feature is the noticeable flattening of multicomponent architectures obtained on properly replacing the phenyl connectors with pyrimidinyl ones (regio-isomer *int*.), as expected. This flattening is revealed by comparing the calculated values of θ_1 for locally analogous ph-based (**Dd1**, **Td1**) and regio-isomers *ext*. of pm-based (**Dd6**, **Td6**) PMMDs ($\theta_1 = 71.8°$ on average) with θ_1 values calculated for regio-isomers *int*. **Dd5** and **Td5** ($\theta_1 = 55.5°$ on average). A similar, but somewhat less pronounced, propensity to flatten is found for the bare pm-An-pm reference species (Table 3) on going from regio-isomer *ext*. (**Ref6**) to *int*. (**Ref5**). Although expected, as a consequence of the decrease of the P/B local steric hindrance, the calculated geometrical impact of pyrimidine replacement for regio-isomer *int*. remains smaller than that obtained when functionalizing the anthracene unit with a phenyl spacer at position $C2^{An}$ (Figure 1) lacking the cumbersome *peri* H atom (that is, $\theta_1 = 33.4°$ for **Dd4** and **Td4**).[14] The structural effect is actually found to be of the same order of magnitude as that computed for a phenyl connection at position $C1^{An}$ of anthracene with only one *peri* H atom (that is, $\theta_1 = 51.8°$ for **Dd3** and **Td3**; Figure 1).[14] Regarding the much less congested B/SC intercomponent linkage, the θ_2 tilt angle remains similar to angular values computed for ph-based species, that is, less than 3°.[14] In the case of regio-isomers *ext*. (**Dd6** and **Td6**), however, θ_2 is found to dramatically increase to approximately 63°. This discrepancy can be ascribed to the larger electrostatic repulsion between the lone pairs of the nitrogen atoms of the pm rings and those of the oxygen atoms of the IN radicals.[37] As a result of this geometrical decoupling about θ_2, it is anticipated that the imino-nitroxide unit is substantially decoupled, including at the electronic/magnetic level, from the photosensitizer, at least in the ground state. Apart from this, only marginal deviations of molecular structures are found with respect to the reference ph-based PMMDs (**Td1** and **Dd1**)[14] and the internal geometry of the IN radicals is not greatly affected by the change of spacer.

Roughly the same trends hold for OV-based PMMDs (**Dd7**, **Dd8**, **Td7**, and **Td8**) as for IN-based polyads. The only noticeable difference stems from the smaller geometrical decoupling about θ_2 computed for regio-isomers *ext*. (**Dd8** and **Td8**: $\theta_2 = 40.05°$ on average versus 63° for IN analogues), which is ascribed to the reduced intercomponent electrostatic repulsion compared to IN derivatives. This finding further substantiates the choice of OV as the more suitable SC for the presently investigated family of PMMDs.

Insights into structural features of lowest THEXI states; case of dyad and triad PMMDs: The two types of conformations computed for the lowest THEXI states of various PMMDs are shown in Figures 4 and 5.

Regio-isomers *int*. (**5** and **7**) and *ext*. (**6** and **8**) clearly show bifurcating behavior subsequent to photoexcitation.

On the one hand, isomers *ext*. retain the same axially distorted conformation as photoexcited ph-based PMMDs. Photoinduced structural changes essentially consist of the overall planarization[38] ($\Delta\theta_n^* = \theta_n^* - \theta_n < 0$) of the modular

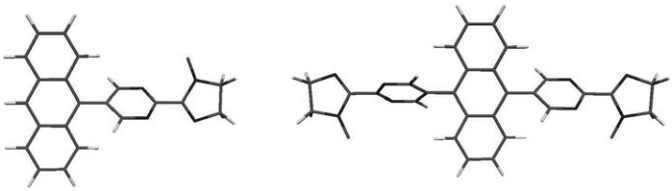

Figure 4. Representative optimized excited-state structures of PMMDs based on pyrimidinyl regio-isomers *ext*.: cases of **Dd6*** (left) and **Td6*** (right); Usual axially distorted conformation.

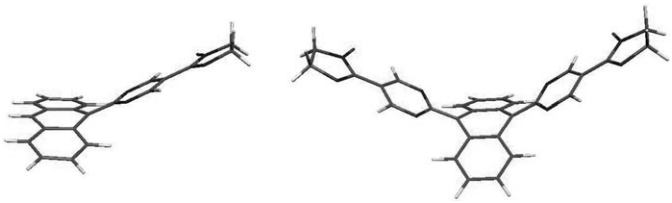

Figure 5. Representative optimized excited-state structures of PMMDs based on pyrimidinyl regio-isomers *int*.: cases of **Dd5*** (left) and **Td5*** (right); Emergent saddle-shaped conformation.

assemblies about interannular bonds along the main molecular axis. This structural relaxation about θ_1 is of the same magnitude as for ph-based reference polyads, that is $\approx -16°$, and of different magnitude about θ_2 depending on whether SC is IN or OV. Typically, $\Delta\theta_2^*$ amounts to about −4° on average for **6*** and ranges from −29° to −39° for **Td8*** and **Dd8***, respectively. The latter discrepancy is due to the above-mentioned differential B/SC intercomponent electrostatic repulsion. The point is that the pyrimidine element remains loosely coupled with both of the SC and P components in the case of regio-isomer *ext*. of IN-based PMMDs (**6**). As a result, the P* core (that is, the central SC) is largely decoupled from the remote radicals through cumulated distortions along the -(θ_1^*)-B-(θ_2^*)- axis, as is the case in the ground state.

On the other hand, for regio-isomers *int*., not only the expected planarization about θ_1 is found to occur with an unprecedented magnitude (θ_1 is virtually zero as far as it can still be defined; see Figure 3), but also the dramatic bending of the whole molecular backbones including the anthryl core is computed, as depicted in Figure 5. This saddle-shaped (equally referred to as butterfly-shaped) structural deformation is reminiscent of that experimentally evidenced (including by X-ray crystallography) for 9,10-bis(1,3-dithiol-2-ylidene)-9,10-dihydroanthracene derivatives[39] as "π-extended TTFs"[40] (TTF = tetrathiafulvalene), tetracyano-9,10-anthraquinodimethane species[41] as "π-extended TCNQ"[42] (TCNQ = tetracyanoquinodimethane), or bis-quinone-anthracene,[43] even though such distorted conformations are in these cases adopted in the ground state (recovering the usual axially distorted geometry upon oxidation or reduction, respectively). The computed structural deformation is also closely akin to that attached to the 9,10-anthracene Dewar valence isomer, and can be characterized by the

 © 2008 Wiley-VCH Verlag GmbH & Co. KGaA, Weinheim

same set of parameters (α, φ' and r; see Figure 3) accordingly.[44]

Clearly, the saddle-shaped distortion of the structure is directly correlated with the planarization about the θ_1 twist angles, and understanding this planarization actually involves the analysis of the molecular orbitals (MOs), which are reported in the Supporting Information for the case of **Dd5** and **Td5** (Figure S I). In particular, for both the dyad and the triad in the lowest THEXI state, one electron is promoted to an orbital (the highest of the singly occupied MOs, SOMOs) displaying a proto-quinoidal pattern that extends over the whole pm connectors. Further confirmation of the formation of a proto-quinoidal form upon photoexcitation is given by the analysis of the structural changes when going from the ground to the excited state. Indeed, typical bond lengths alternation (BLA) patterns are found for both **Dd5*** and **Td5***, involving the whole An-pm and pm-An-pm moieties, respectively (Supporting Information; Figure S II).

Among the salient excited-state structural features of regio-isomers *int.*, the shortening of all interannular bond lengths when the saddle-shaped distortion occurs is noticeable. 1) For P-B linkages bond length reductions are 0.045 and 0.048_5 Å on average within IN- and OV-based polyads, respectively; 2) for B-SC linkages bond length variations are only 0.012_5 Å (IN-based) and 0.013_5 Å (OV-based) on average, but the corresponding $\Delta\theta_2$* variations are also very small as the B and SC elements are already roughly coplanar. At least in case 1, the shortening of intercomponent bonds can be straightforwardly ascribed to an increase of their double-bond character correlated with the overall planarization (essentially involving θ_1) of the molecular architectures. Again, this observation is indicative of an extension of the π-delocalized system also involving, to some extent, the terminal SCs. In this regard, it is noteworthy that although the excited-state shortening of the interannular distance is virtually the same for **Dd5*** and **Td5***, the amplitude of the planarization about θ_1 (Table 1) is significantly more pronounced for the latter triad ($\Delta\theta_1^* = -58.9°$ to give 0.4°) than for the former dyad ($\Delta\theta_1^* = -40.1°$ to give 11.6°). Correlatively, the saddle-shaped distortion is more pronounced in **Td5*** than in **Dd5***. This difference is indicative of the onset contribution of an extended (quinoidal) wire-like framework mediated by the distorted An backbone. This is a synergistic effect revealing the delocalized nature of the electronic perturbation between the two pyrimidinyl subdivisions across the central ring of An.

For photo-promoted axially distorted regio-isomers *ext.*, whose planarization about θ_1 and θ_2 is partly impeded, less pronounced bond shortenings are computed: 1) 0.014_5 and 0.020_5 Å on average for the P-B linkage; and 2) 0.002 and 0.002 Å on average for the B-SC linkage within IN- and OV-based polyads, respectively.

Insights into structural features of lowest THEXI states of [B-P-B] reference assemblies; the special case of [pm-An-pm]$_{int}$* (Ref5*): There are two conformations that can be computed for the regio-isomer *int.* of 9,10-dipyrimidinyl-anthracene (Figure 2) in its triplet state ^{3}[pm-An-pm]$_{int}$ (**Ref5***; Table 3). Indeed, depending on whether the starting geometry to be optimized is axially distorted or saddle-shaped, the corresponding triplet lowest THEXI state obtained is axially distorted or saddle-shaped, respectively. However, frequency analysis of these stationary points gives a small and imaginary value for the axially distorted geometry, whereas a real frequency is found for the saddle-shaped distortion; moreover, the saddle-shaped conformation is calculated to be more stabilized than the other geometry by approximately 5 kcal. In other words, the potential energy surface (PES) is rather flat (see the General Comments, below) as indicated by the small absolute values of the frequencies, and only the saddle-shaped conformation corresponds to a genuine energy minimum. It remains intriguing that structure optimization of the axially distorted geometry upon change of spin multiplicity does not lead directly to the minimum, whereas this alternative saddle-shaped geometry of the lowest THEXI state is correctly computed when spin carriers (SCs) are appended to the P-B and B-P-B assemblies (regio-isomers *int.* of dyads and triads). Experiments will reveal to what extent this minimum remains hidden in the real world, that is, to what extent the actual presence of an intramolecular persistent source of paramagnetism is mandatory to reveal the saddle-shaped excited-state distortion.[16]

With respect to the regio-isomer *ext.* of the B-P-B assembly (**Ref6**; Figure 2 and Table 3), the only geometry computed for the lowest THEXI state is the slightly planarized ($\Delta\theta_1^* = -12.6°$ to give 62.5°) axially distorted conformation, as expected.

Insights into structural features of lowest THEXI states of the proto-triads (HTD*n*): The above-reported findings further support the hypothesis that persistent radicals play a role in the saddle-shaped distortion by easing or assisting conformational change. To delineate more clearly this contribution, it was therefore interesting to investigate the behavior of regio-isomers *int.* of [B-(θ_1)-P-(θ_1)-B-(θ_2)-SC] proto-triad species (**HTd*n*** type; Figure 2 and Table 4) comprised of only one persistent radical (oxoverdazyl).

As expected, both structures are axially distorted in the ground state. Also, they both show, to different extents, the saddle-shaped distortion in their relaxed lowest-lying excited state (see Figure S III in the Supporting Information), which is accompanied by the expected respectable shortening of the P–B bond(s) by around 0.047 Å on average (when B = pm). The distortion involves the free terminal B extension if it is a pyrimidinyl ring (θ_1 about $C1^{Pm}$–$C10^{An}$ $\approx 0°$ within **HTd71***), but an axially distorted conformation is found when the free dangling B extension is a phenyl ring (**HTd72***). This observation clearly indicates that there exists a direct inter-branch communication, probably supported by an emerging π-delocalized system (namely [-B-(θ_1)-P-(θ_1)-B-], with $\theta_1 \approx 0°$) in the saddle-shaped conformation. Beyond revealing the long-range influence (most likely of electronic nature) of the single persistent SC, which even propagates across the triplet of An, this feature is anticipat-

 © 2008 Wiley-VCH Verlag GmbH & Co. KGaA, Weinheim

Table 4. Selected structural parameters computed for verdazyl derivatives **HTd71** and **HTd72** in the ground and excited (*) states as a function of the overall spin. Distances in Å, angles in degrees. For labeling system refer to Figures 2 and 5.

	HTd71 $S=1/2$	**HTd71*** $S=3/2$	**HTd72** $S=1/2$	**HTd72*** $S=3/2$
dC10^{An}–C1$^{Pm/Ph}$	1.490	1.448	1.494	1.486
dC9^{An}–C1^{Pm}	1.487	1.436	1.486	1.438
dC4^{Pm}–C1^{OV}	1.470	1.457_5	1.470	1.455
θ_1(pm/ph)	62.7	(0.8)	77.0	64.5
θ_1(OV)	57.4	(0.7)	56.4	(0.70)
θ_2(OV)	2.1	0.0	0.6	0.0_5
$\varphi=180-\varphi'$	(0)	82.1	(0)	npd[a]
α_1/α_2	(0)	30.0	(0)	27.5
dC9^{An}–C10^{An}/r	2.850	2.828	2.859	2.873

[a] npd: not properly defined.

ed to have a significant impact on the magnetic couplings of the various (transient and persistent) magnetic sites when θ_2 is also roughly 0°, that is, in most cases.

Close analysis of the small, but significant, variations of the C9^{An}-C10^{An} distance (corresponding to parameter r for saddle-shaped conformation; Figure 3, and Tables 1, 2 and 4) also reveals interesting structural features of various excited states. Concerning the relaxed geometries of photoexcited regio-isomer *ext.*, dC9^{An}–C10^{An} is equal to 2.858 and 2.888 Å on average for **Dd(6/8)*** and **Td(6/8)***, respectively. Very similar structural features are computed for axially distorted excited states of ph-based PMMDs that is, 2.851 and 2.895 Å on average for **Dd(1/2)*** and **Td(1/2)***, respectively.[14] On the contrary, in the case of regio-isomers *int.*, the anthracene cross section (r) does not increase by 1% on going from excited dyads to excited triads, but decreases by 0.85%, instead. Indeed, r attached to butterfly conformation is equal to 2.856 and 2.832 Å on average for **Dd(5/7)*** and **Td(5/7)***, respectively. Interestingly, it is found that **HTd71*** ($r=2.828$ Å) is therefore preferably affiliated to the triad species, but **HTd72*** ($r=2.873$ Å) is more akin to the dyad species. These trends indicate that the hypothesized extension of the π-delocalized system in the saddle-shaped distorted excited states basically has its origin in the bending of the anthracene backbone about its central ring in the proper regio-isomer *int.*

Insights into the magnetic behaviors of the ground and excited states: Assessing the molecular properties of the PMMDs inevitably involves the analysis of their electronic features, all the more because photo-induced structural changes (planarization and saddle-shaped distortion), which are undoubtedly of electronic origin, are also determining factors for exchange couplings according to known magneto-structural correlations.

Analysis of the spin density maps: Spin density (SD) maps of open-shell π-conjugated molecules are highly informative when dealing with intramolecular magnetic properties. Analysis of the matching or mismatching of polarization patterns attached to various SD-perturbing magnetic sites allows insights into the nature (ferro/antiferro) of the prevailing exchange couplings, regardless of whether ground or excited states are considered.[14] As the polarization patterns are essentially supported by the π-systems of various components (P, B, and SC), intercomponent linkage and attached dihedral angles (θ) are worth being considered as "defects" likely to alter the propagation of polarization patterns by diminishing inter-ring π-overlapping. Moreover, the magnitude of an exchange coupling constant J attached to two interacting magnetic sites largely depends on the critical absolute values of (α–β) net electron spin contributions (that is, atomic spin populations: ASPs) located at either side of each intervening interannular bond.[45] Therefore, the smaller the value of θ, the larger the value of J, accordingly.[14]

SD maps of all PMMDs have been computed for both their ground and lowest THEXI states. Regarding axially distorted ground states, SD patterns are found to be virtually the same as those computed for ph-based PMMDs; they are thoroughly analyzed in ref. [14] The only noticeable deviation concerns regio-isomers *ext.* **6** (and to a lesser extent polyads **8**). In this case, almost no perturbation (namely polarization) of the SD is found over the anthracene core (Supporting Information, Figure S IV), as a result of the unusually pronounced decoupling of the remote SC(s) about θ_2 (see above).

Regarding the excited states, SD maps computed for IN-based PMMDs (also representative of SD patterns of OV-based species) are given in Figures 6 and 7.

When comparing the patterns of SD distributions over the An backbone for axially distorted (Figure 6) and saddle-shaped (Figure 7) excited-state conformations, it clearly ap-

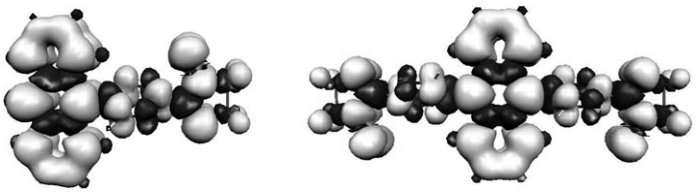

Figure 6. Spin-density patterns (contour value 5×10^{-4} a.u.) computed for axially distorted photoexcited regio-isomers *ext.*; the representative cases of **Dd6*** ($S=3/2$; left) and **Td6*** ($S=2$; right).

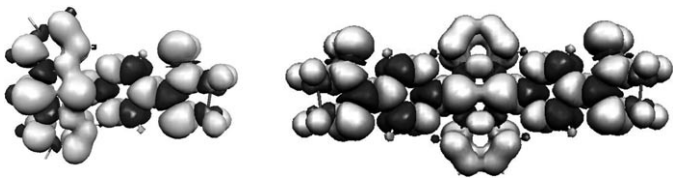

Figure 7. Spin-density patterns (contour value 5×10^{-4} a.u.) computed for saddle-shaped photoexcited regio-isomers *int.*; the representative cases of **Dd5*** ($S=3/2$; left) and **Td5*** ($S=2$; right).

© 2008 Wiley-VCH Verlag GmbH & Co. KGaA, Weinheim

pears that they are significantly different. In the former case, the SD distribution over the polyacene backbone is barely influenced by the presence of one or two B-SC branches regardless of the nature of B (that is, ph[14] or pm regio-isomer *ext.*, Figure 6). In the latter case, not only is a dramatic alteration of the SD pattern of the anthracene triplet computed, but the perturbation is also shown to be different depending on whether the An core bears one or two B-SC branches (Figure 7).

The most important changes noticed on going from axially distorted to saddle-shaped distorted geometries concern the central ring of An. 1) The sign of (α–β) net electron spin contributions lying on the shared internal bonds of laterally fused rings becomes the same as that of the SD lying on vertices (rims)[46] and potentially bearing substituents. 2) Some spin density arises across the bent central ring between atoms $C9^{An}$ and $C10^{An}$, suggesting the onset of the formation of a bond similar to that encountered in Dewar anthracene valence isomers.[44] The point is that, together with the shortening of the P–B bonds showing partial double-bond character, the central ring of anthracene displays partly quinonoid features upon saddle-shaped distortion, in accordance with previous issues (see also Figure S II).

Finally, it is worth noting that, in the case of "extended-dyad" **HTd71*** (Figure 8), the presence of the free terminal pyrimidinyl ring noticeably contributes to making the SD distribution pattern more akin to that of **Td7*** (and **Td5***) than to the one of the bare dyad **Dd7*** (and **Dd5***). The dangling pyrimidine somehow equalizes (averages) the ASP at key $C10^{An}$ and $C9^{An}$ positions by evening up the SD distribution over An (Figure 7 and 8). The absolute value of ASP located at $C9^{An}$ in **HTd71*** (ASP = 0.63) is then made significantly larger than that calculated for strongly dissymmetric **Dd7*** ($ASP(C9^{An}) = 0.56$) or **HTd72*** ($ASP(C9^{An}) = 0.60$). This issue again highlights the effective function that B elements may have within PMMDs.

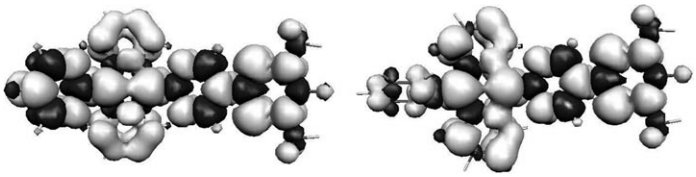

Figure 8. Spin-density patterns computed for **HTd71*** (left) and **HTd72*** (right) ($S = 3/2$; contour value 5×10^{-4} a.u.)

Insights into electronic structures of ground and lowest THEXI states: Whether from excited-state planarization or from emergent saddle-shaped distortion, there is every indication that the spatial expanse of the π-conjugated systems most probably changes when PMMDs are going from their ground state (GS) to their high-spin lowest THEXI state (LTS). These issues naturally drive us to compute the energy difference between these states ($\Delta E = E(\mathrm{LTS}) - E(\mathrm{GS})$) for various polyads (Table 5).

Table 5. Total energy differences (ΔE, in eV) computed for: **pm-An-pm** isomers (singlet (S_0, $S=0$) to triplet (T_1, $S=1$)), **Dd5**, **Dd6** , **Dd7**, **Dd8** together with **HTd71** and **HTd72** (doublet (D_0, $S=1/2$) to quartet (Qr_1, $S=3/2$)), and **Td5**, **Td6** , **Td7** and **Td8** (triplet (T_0, $S=1$) to quintet (Qn_1, $S=2$)).

	Regio-isomers *int.*							Regio-isomers *ext.*				
ΔE[a]	**Ref5**[b]	**Dd5**	**Dd7**	**Td5**[c]	**Td7**[c]	**HTd71**	**HTd72**	**Ref6**	**Dd6**	**Dd8**	**Td6**[c]	**Td8**[c]
S_0-T_1	1.47							1.69				
D_0-Qr_1		1.55	1.60			1.36	1.53		1.74	1.73		
T_0-Qn_1[b]				1.25	1.29						1.68	1.71

[a] Structure optimized at LANL2 level and energy evaluated at LANL2 level. Energy gaps are calculated between relaxed excited and ground states. [b] Reported value is attached to saddle-shaped conformation; for hypothetical axially distorted geometry, $\Delta E = 1.62$ eV. [c] For triad species, the triplet ground-state (T_0) has been considered instead of the BS state ($m_S = 0$) virtually lying at the same energy ($J_{GS}/k_B < -2$ K) to allow for a direct comparison with the reference molecules and dyads.

Clearly, smaller ΔE values are computed when PMMDs undergo excited-state saddle-shaped distortion, as expected. Moreover, among the regio-isomers *int.*, ΔE values attached to triad species (**Td5** and **Td7**) are significantly smaller (by ≈20%) than ΔE values calculated for affiliated dyads (**Dd5** and **Dd7**). This trend can be straightforwardly ascribed to a greater extension of the π-conjugated systems within excited triads than within excited dyads with respect to their loosely π-conjugated axially distorted (θ_1, θ_2) ground state geometries. Interestingly, also, the energy gap calculated for **HTd71** is found to be close to that of **Td7**, whereas ΔE associated with **HTd72** is estimated to be roughly the same as that of **Dd7**. This differential "electronic affiliation" for the **HTd** model species gives further evidence that the free dangling pyrimidinyl subdivision (B) merely plays the role of a π-extending group when properly oriented (even though deprived of a dangling SC).

Enhanced π-delocalization in the excited state is likely to impact (increase) markedly the magnitude of the superexchange coupling constants (J_{ES}). The fact that the energy gap is smaller in distorted triads than in distorted dyads clearly indicates that the π-conjugated system does involve both branches[47] across the distorted anthracene (as previously inferred), which loses part of its aromaticity as such.[40] Therefore, the overall picture we get is consistent with a light-triggered switching of the preferential axis for π-delocalization (Figure 9) from the An backbone in the axially distorted ground state to the perpendicular two [B-SC]-branches system, including the bent An central ring, in the saddle-shaped excited state ($\theta_1 \approx \theta_2 \approx 0°$; Tables 1, 2, and 4).

As a consequence of the inter-branch direct communication of remote SCs, J_{ES} could no longer be derived from the magnetic behavior of dyads (for regio-isomers *int.*), which are no longer fully relevant models. In this case, J_{ES} should be assessed using actual saddle-shaped distorted triads (see below).

 © 2008 Wiley-VCH Verlag GmbH & Co. KGaA, Weinheim

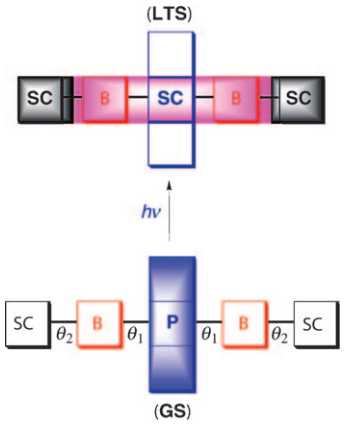

Figure 9. Switching of the preferential axis for π-delocalization within the cruciform regio-isomer *int.* upon photoinduced formation of the saddle-shaped distorted lowest THEXI state (LTS).

Quantifying exchange-coupling constants: At this stage, it is worth reminding that ground-state magnetic couplings (between remote SCs) are calculated on triad models (**Td*n***), whereas excited-state magnetic couplings (essentially lying between each remote SC and the nexus photo-promoted triplet state of the An core) are normally assessed on dyad models (**Dd*n****) in their lowest THEXI state (Scheme 1).[14] Calculated values for exchange coupling constants (J/k_B) of various molecules in both their ground states and lowest excited states are gathered in Table 6.

Accounting for the magnetic behavior of PMMDs is straightforward on the basis of the above-identified structural and electronic features, as intramolecular magnetic interactions are essentially mediated by the π-systems.

Ground-state magnetic couplings (J_{GS}, Table 6) computed for regio-isomers *int.* (**5** and **7**) are of the same order of magnitude as those found for ph-based PMMDs (**Td1**, **Td2**, **Td3**, and **Td4**; Figure 1).[10,14] However, they are significantly larger than those calculated for regio-isomers *ext.*, in particular for **Td6**, which displays pronounced and cumulated geometrical decouplings about the θ_1 and θ_2 torsion angles. Actually, in the latter case, the energy computed for the BS state ($m_S=0$; antiferromagnetic coupling of the SCs) is exactly degenerate with that of the triplet state ($S=1$; ferromagnetic coupling of the SCs). For **Td6**, in the ground state, the radicals behave as two independent magnetic sites ($J_{GS}/k_B=0$ K, Table 6), in agreement with issues derived from the spin density maps computed for **Dd6** and **Td6** (see the Supporting Information, Figure S IV).

Regarding the magnetic behavior in the excited state, ferromagnetic interactions ($J_{ES}>0$) are in all cases computed for the lowest THEXI states, thereby confirming the high-spin nature of photoexcited PMMDs studied herein, that is, the photo-induced intramolecular spin alignment. According to previous issues, and more especially possible long-range interaction of remote SCs when saddle-shaped distortion emerges, it is worth referring to J_{ES} values computed for the excited triads (**Td*n****) rather than for the formally affiliated excited dyads (**Dd*n****) in the case of regio-isomers *int.* Thus, on the whole, J_{ES} couplings span more than one order of magnitude: from +30 K (**Dd6***) to ≈+600 K (**Td7***).

In the case of **Dd6***, the decoupling of the IN unit from the triplet photosensitizer is the largest when compared to other members of the family with the same connection scheme, including **Dd8** (planarized about θ_2 in the ES) and also ph-based polyads. This magnetic decoupling is essentially owed to the larger value of θ_2: 58° (after planarization) versus less than 1° for other PMMDs. As a result, the superexchange pathway is less efficient and the value of magnetic exchange coupling (J_{ES}/k_B) is the smallest of the series: +30 K for **Dd6*** versus +222 K for **Dd8*** and +150 K on average for **Dd1*** and **Dd2***.[14]

On the other hand, the situation is completely different for the photoexcited regio-isomers *int.*, as the distortion of the anthracene combined with the enhanced localization of the spin density (that is, enlarged ASP value) at key positions $C9^{An}$ (for P*) and $C1^{pm}$ (for B) allows a stronger excited-state exchange interaction (see Figure 7).[14] Estimated J_{ES} values are much greater than those hitherto reported for similar molecules. Typically, J_{ES}/k_B is +562 K on average for regio-isomers *int.*, on the basis of data calculated for excited dyad dissymmetric models. Comparison of J_{ES} values computed for **Dd5*** and **Dd7*** clearly shows that OV is a more suitable spin carrier than IN, as already observed.

Analysis of the outcomes associated with PMMDs of type **7** (OV-based derivatives) allows 1) assessment of the impact of the saddle-shaped distortion, as such, on magnetic behaviors; 2) derivation of the magnitude of the anticipated alteration of the J_{ES} values on passing from excited dyads to excited triads for the purposes of computational modeling. Thus, close inspection of Table 6 reveals that the calculated J_{ES} values continuously *decrease* on going from the **Dd7*** model to **Td7*** according to the following sequence: **Dd7*** ($J_{ES}/k_B=+656$ K) ≈**HTd72*** ($J_{ES}/k_B=+651$ K) > **Dd7T*** ($J_{ES}/k_B=+629$ K) > **HTd71*** ($J_{ES}/k_B=+605$ K) > **Td7*** ($J_{ES}/k_B=+596$ K). Interestingly, on the basis of the structural

Table 6. Computed intramolecular exchange coupling constant in the ground state (J_{GS}/k_B, in K) and in the excited (*) state (J_{ES}/k_B, in K) for compounds **5**, **6**, **7** and **8**. Negative *J* values imply antiferromagnetic couplings. **Dd7T*** refers to **Dd7*** frozen in the saddle-shaped distorted geometry of **Td7***. **Dd8T*** refers to **Dd8*** frozen in the axially distorted geometry of **Td8***.

	Regio-isomers *int.*								Regio-isomers *ext.*					
	Td5	**Td7**	**Dd5***	**Dd7***	**Dd7T***	**Td7***	**HTd71***	**HTd72***	**Td6**	**Td8**	**Dd6***	**Dd8***	**Dd8T***	**Td8***
J_{GS}/k_B[a]	−1.3	−1.7							0.0	−0.1				
J_{ES}/k_B[a]			+469	+656	+629	+596	+605	+651			+30	+222	+204	+201

[a] Values computed as in ref. [14].

© 2008 Wiley-VCH Verlag GmbH & Co. KGaA, Weinheim

and electronic insights hitherto gained, one can note that the local level of symmetry (including inseparable correlative expansion of the π-system) about the anthracene core of the models continuously *increases* on going from **Dd7*** to **Td7*** as follows: **Dd7*** ≈ **HTd72*** < **Dd7T*** < **HTd71*** < **Td7***. Moreover, it is worth noticing that, basically, regardless of the actual spatial expanse of the quinonoid pattern over the [-B-(θ_1)-P-(θ_1)-B-]* fragment, the SD polarization scheme of the excited state is not altered and remains favorable to ferromagnetic interaction of the magnetic sites (SCs and/or P*). This is all the more true in that direct interbranch communication is partly ensured by the onset of bond formation between atoms $C9^{An}$ and $C10^{An}$, which moreover support the ASP values of the same sign (see Figure 7).

Brought together, these issues clearly indicate that the very nature of the adverse effect of the wire-like quinonoid system is not a hypothetical antiferro contribution,[48] but actually stems from its overall delocalized character, which results in the averaging of the local ASPs, including at key sites such as intercomponent P/B (and maybe also B/SC) linkages (Figure 9). Regardless of the probable low weight of the quinonoid electronic contribution, the effect is anticipated to be rather moderate because PMMDs are relatively compact with respect to the number of active magnetic sites. Therefore, partial quinoidal delocalization can absolutely explain the slight lowering of J_{ES} computed for the saddle-shaped triads as compared to that assessed on the corresponding (similarly distorted but more localized) model dyads. All in all, this identified drawback of delocalization, namely the averaging of ASPs,[49] is trivial compared with the overall largely improved ferromagnetic interaction of the magnetic sites that has been made possible.

Beyond making questionable the full relevance of excited dyads as models for assessing J_{ES} operative in photoexcited triads, the enhanced π-delocalization correlative to saddle-shaped distortion also relates back to a genuine molecular feature of photoexcited regio-isomer *int.*, which is truly likely to make the actual ferromagnetic coupling within excited triads smaller than in the affiliated excited dyads. When no such contribution exists, as is the case for usual axially distorted photoexcited PMMDs,[14] J_{ES} values computed for related **Dd*n*** and **Td*n*** are very close, further legitimizing the use of dyads for modeling J in the excited state.[14] Thus, in the illustrative case of compounds **8**, $J_{ES}/k_B = +222$ K for **Dd8*** ($\theta_2 = 0.4°$) versus $+201$ K for **Td8*** ($\theta_2 = 11.5°$), whereas for **Dd8*** frozen in the geometry of **Td8*** (i.e., **Dd8T***; $\theta_2 = 11.5°$) J_{ES}/k_B amounts to $+204$ K (Table 6) that is, virtually the same value as for the related triad within the range of computational accuracy. On the contrary, J_{ES}/k_B values computed for **Td7*** and **Dd7T*** with the same saddle-shaped distorted geometry were significantly different: $+596$ and $+629$ K, respectively. On the whole, the overestimation of J_{ES} when calculated with dyad models remains small when present. **Dd*n*** is a relevant model to calculate J_{ES} associated with affiliated triad species provided that significant structural differences between **Dd*n*** and **Td*n***, especially the dihedral angles θ_1 and θ_2, are taken into account.

To summarize, the presence of strongly spin-polarizing remote radical(s) together with a proper P-B-SC connection scheme (including the directional pyrimidinyl connector B, regio-isomer *int.*) and a convenient balance of P/B steric interplay (*peri* H atoms versus nitrogen lone pairs) are all responsible for the changes in geometry and electronic structure emerging in the excited state (saddle-shaped distortion). This light-induced upheaval gives rise to a strong ferromagnetic interaction (≈ +600 K) between the triplet excited state of An and the doublets of the dangling radicals, which corresponds to a dramatic functional improvement of the PMMDs as J_{ES} calculated for ph-based PMMDs is only +150 K on average.[14]

Qualitative insights into photoinduced intramolecular charge redistributions: As far as we know, "butterfly" distortions occurring in the excited state and hypothesized to be associated with Dewar valence isomer formation are actually very scarce. Examples essentially concern photoactive donor-acceptor molecules designed to undergo photoinduced twisted intramolecular charge transfer (TICT),[50] and more particularly tetrafluoro analogues of *N,N*-dimethylaminobenzonitrile (DMABN).[51] In this case, unusual excited-state behavior (compared to parent DMABN) is indeed ascribed to the intervening distorted conformation (towards the Dewar isomer), assumed to originate from the combined contributions of 1) increased steric hindrance between the two methyl groups of the amine moiety and the proximal fluorine atoms of the fluorinated benzene core (dC-F ≈ 1.3 Å versus dC-H = 1.08 Å in native DMABN); and 2) enhanced ICT due to the strengthened electron-withdrawing ability of the tetrafluoro-benzonitrile acceptor moiety.[51]

Contrary to the excited state, ground state conformational switching between the (neutral) butterfly-shaped conformation and the (charged) axially-distorted conformation is quite common,[39,42] but is not supposed to rely on the onset of the formation/destruction of the Dewar valence isomer. Hitherto reported examples are usually redox-triggered. For instance, it has been shown in so-called extended-TTF that the laterally-fused polyacenic unit (namely, anthracene) can act as an acceptor[52] with respect to the dangling dithiole (donor) units. The saddle-shaped distorted geometry of the neutral form of extended-TTF originates from the balance between the opposite contributions of 1) the quinonoid (electronic) structure (likely to make the overall molecular architecture more planar); and 2) the intramolecular steric hindrance located between the sulfur atoms of donors and the *peri* hydrogen atoms of polyacene (likely to impede molecular flattening). Upon oxidation of the two donors, the charge-transfer (CT) component is withdrawn and the extended-TTF dication adopts the axially distorted geometry comprised of the planar polyacene core linked to canted (almost perpendicular) rings of aromatized dithiolium moieties (Figure 10a).[39] Similar structural switching from the

 © 2008 Wiley-VCH Verlag GmbH & Co. KGaA, Weinheim

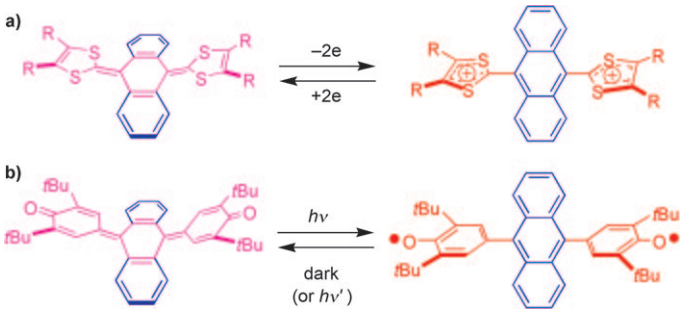

Figure 10. a) Reversible redox-driven structural switching of "extended TTF" according to ref. [39]. b) Reversible photochemical/thermal switching of dibenzoannulated 3,5,3",5"-tetra(*t*-butyl)-*p*-terphenoquinone according to ref. [43].

saddle-shaped (neutral) form to the axially-distorted conformer can also be obtained upon (two-electron) reduction, as in the cases of 11,11,12,12-tetracyano-9,10-anthraquinodimethane[42] and extended quinones reported by Oda.[43] Interestingly, in the latter case, the conformational change can also be monitored by photochemical-thermal means, involving the neutral saddle-shaped conformer and the axially-distorted diradical species (Figure 10b).[43] It is also noteworthy that the butterfly distortion is observed despite the significant congestion about the linkages between the An core and the quinone branches, which is virtually identical to that present in ph-based PMMDs (**Td1** and **Td2**) as well as in regio-isomers *ext.* of pm-based PMMDs (**Td6** and **Td8**).

In light of the above-mentioned examples of switchable conformations from saddle-shaped to axially-distorted geometries, the interplay between redox-driven processes (whether or not light-induced) and local steric restraints (congestion) about the linkage of the donor/acceptor redox partners clearly appears to be a determining factor. Therefore, it is worthwhile investigating to what extent similar intermingled contributions may also exist in the saddle-shaped distorted photoexcited regio-isomers *int.* of PMMDs. This is all the more advisable in that each of the P, B, and SC components of the PMMDs is potentially redox active and ambivalent towards electron-donating or accepting properties (depending on the redox partners). Anthracene in its triplet excited state can either be an electron-donor[11] or an electron-acceptor,[53] as illustrated when photoinduced symmetry breaking occurs within bianthryl.[50,54] Regarding the spin carriers (OV and IN), which have roughly the same redox properties, they can behave as either weak donors or acceptors because they are expected to be quite easily oxidized or reduced to the corresponding closed-shell cations/anions.[37,55–58] Regarding the pyrimidinyl connector B, which is basically known as a π-accepting fragment,[21] it can also play the role of a donor with respect to anthracene when linked to (bi)pyridyl groups.[59]

Hence, the question was raised whether (light-triggered) intramolecular charge-transfer (ICT) could occur and take an active part in the structural upheaval we found. The variations of the Mulliken charges (in electron units) attached to the various P, B, and SC components of PMMDs on going from the GS to the lowest THEXI state (LTS) are given in the Supporting Information (Table SIV). This type of charge analysis was chosen mainly for the sake of consistency with the discussion of ASPs.[60] However, the magnitudes of charge variations are small so that only qualitative issues could safely be derived (Figure 11).

Within [B-P-B] isolated assemblies (**Ref5** and **Ref6**), the redox behavior of ^{3}An* is directed to that of an electron acceptor or an electron donor depending on whether anthracene is linked to the carbon atom of the pyrimidine ring *ortho* to both heterocyclic nitrogen groups (regio-isomer *int.*) or to the carbon atom of the pyrimidinyl *meta* to both of the heterocyclic nitrogen atoms (regio-isomer *ext.*), respectively (Figure 11; Table SIV). It is noteworthy that for regio-isomer *int.* (**Ref5***), in the case of a hypothetical axially-distorted LTS, basically the same trend for charge redistribution as in the case of saddle-shaped distortion is computed (Table SIV). Besides suggesting that mere regio-isomerism is probably sufficient to govern the redox activity of ^{3}An*, this finding further substantiates previous issues ascribing to the [B-P-B] core assembly the origin of the saddle-shaped distortion within PMMDs.

On the one hand, the charge redistribution (that is, electron delocalization) is negligible within PMMDs based on phenyl as the B element (Figure 1).[14,61] On the other hand, ^{3}An* is systematically slightly oxidized in the case of pm-based PMMDs regardless of their regio-isomerism, and conversely to reference species (**Ref5** and **Ref6**) lacking the SCs (Table SIV). Thus, SC components behave as electron acceptors rather than electron donors. The fact remains, nonetheless, that regio-isomerism associated with the pyrimidine is also likely to impact the redox properties of the appended SCs, as judged from literature data. For instance, the reduction potential of OV is shifted from −1.25 V[55] to −0.85 V[56] (vs. SCE in MeCN)[62] depending on whether this radical is linked to the carbon atom *ortho* to both pyrimidino nitrogen atoms (as in the case of PMMDs regio-isomers *ext.*) or to a phenyl (e.g., as in **Dd2** and **Td2**; Figure 1), respectively. It is therefore anticipated that dangling SCs will behave as stronger electron acceptors within PMMDs regio-isomers *int.* than in PMMDs regio-isomers *ext.*, all the more since θ_2 systematically approaches 0° in the former. These issues are consistent with tendencies derived from the data of Table SIV. On the whole, the [B-(θ_2)-SC] branches apparently behave as weak electron-accepting assemblies and P* as weak light-triggered electron donors (Figure 11).

For regio-isomers *ext.*, ICTs are essentially confined to the [P-B] and [B-P-B] cores of dyad and triad species. The magnitude of ICTs within photoexcited triads is twice as large as that of ICTs occurring within related dyads. Addition of the contributions indicates that each functional subsystem (P/B/SC) undergoes the same electronic effect regardless of the composition of the overall assembly (whether a dyad or a triad). Hence, the picture drawn from these issues is consistent with the localized description of PMMD assemblies at the electronic level, as far as regio-isomers *ext.*

 © 2008 Wiley-VCH Verlag GmbH & Co. KGaA, Weinheim

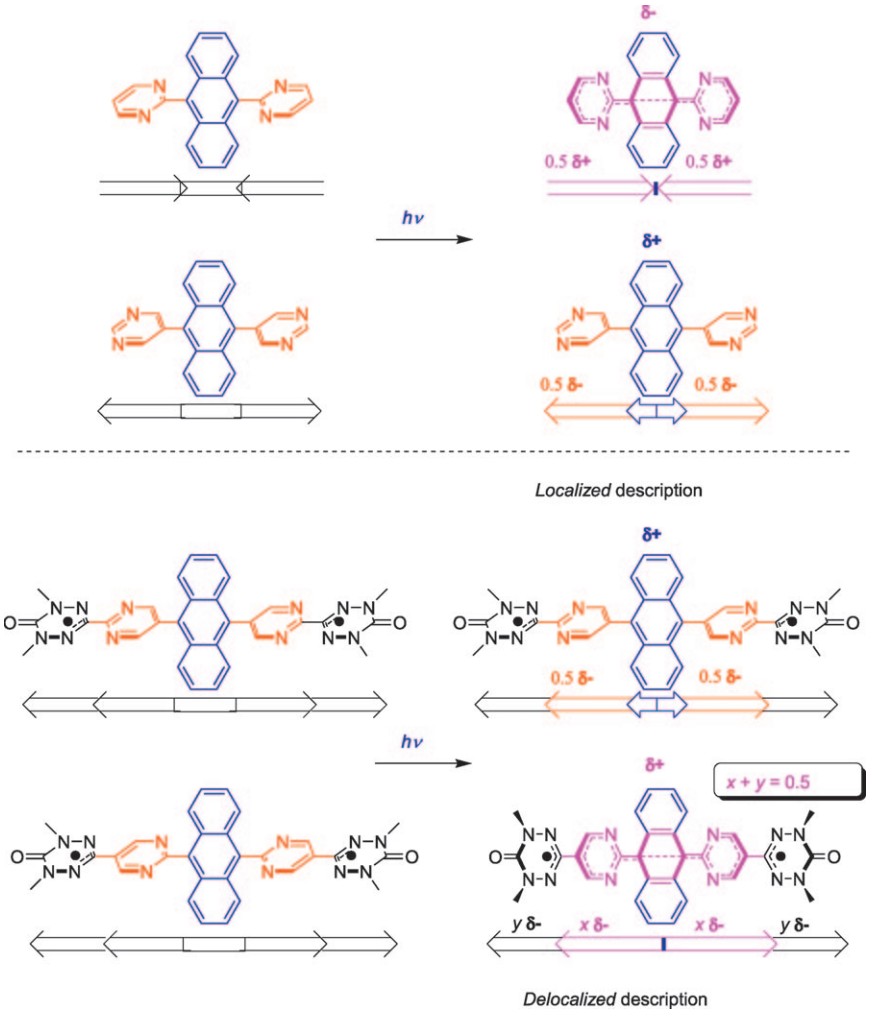

Figure 11. Pictorially represented qualitative charge variations on going from the GS to the LTS (Table SIV). Arrows indicate polarization direction of various functional elements at the electronic level and partial ICT in the excited state.

are concerned (Figure 11). Conversely, for regio-isomers *int.*, various subsystems behave differently depending on whether they are embedded within dyads or triads (Table SIV). In this regard, the case of the B element is particularly informative. Whereas almost no electron density seems to be shifted onto intervening B subsystems within triads, part of the electron density originating from ^{3}An* settles of the B units within the affiliated dyads. On the whole, however, there are net (little and partial) electron transfers (ICTs) from P* to remote SC(s) in both dyads and triads. Thus, B somehow plays the role of an electron wire within triads, but acts as an electron-accepting subunit in the case of dyads. These findings are consistent with the previously inferred small contribution of the onset formation of a quinoid π-delocalized system, which is significantly more developed within the saddle-shaped distorted triads than in the corresponding dyads (Figure SII). In addition to favoring charge separation ([P$^+$-B-SC$^-$]*; Figure SV) that is, the reduction of dangling SCs, this quinoid pattern is also likely to support back transfer of electron density from the reduced remote sites (SC) to the core by virtue of limiting canonical resonance forms (Figure SV). Although small, this balanced contribution of the resonance forms can account for both the smaller net ICTs computed for excited triads than for related dyads, and the averaging of the redistributed charges, which are made more evenly shared between the P* and SC extremities of the B electron wires within triads. This feature is reminiscent of the previously identified equalization of local ASPs upon the averaging of SD perturbation over the extended delocalized system associated with saddle-shaped distortion, especially in triad species. Brought together, these issues indicate that regio-isomers *int.* fit a delocalized description of their lowest THEXI state as far as their electronic features are concerned, in particular for triad molecules (Figure 11 and SV).[63]

Finally, for PMMD regio-isomers *int.*, it is worth noting that structural relaxation towards the saddle-shaped conformation is computed although ICT direction is inverted as compared to **Ref5*** (Figure 11 and Table SIV), which is found to undergo the same distortion. This observation further confirms the fact that there is no simple relation between the direction of ICTs (P*→B(SC) or (SC)B→P*) and the formation of the saddle-shaped distortion. Rather, the increase of electron density about key interannular linkages to driving planarization appears to be the actual determining factor, regardless of the origin of incoming ASP. Accordingly, saddle-shaped distortion is indeed also obtained within **Ref5** upon mono-electronic reduction.[64] Spin density maps computed for **Ref5** cation and anion (Figure 12) revealed that only in the case of the reduced species is sufficient SD perturbation (and more especially ASP) localized about intercomponent linkages, moreover filling the bonding proto-quinoidal LUMO, as in the case of the photo-promoted electron in the lowest THEXI state of **Ref5*** (Figure SVIII; Supporting Information).

Together, these observations indicate that the determining difference between regio-isomers *int.* and *ext.* of PMMDs is basically the small differential steric congestion about the P/B linkage (θ_1), beyond the differences attached to the intrin-

 © 2008 Wiley-VCH Verlag GmbH & Co. KGaA, Weinheim

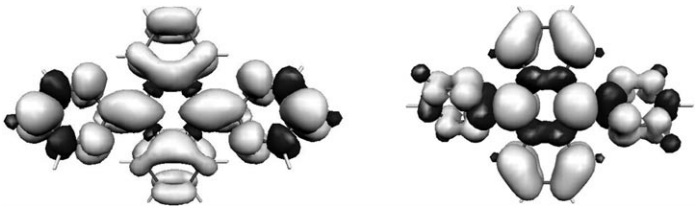

Figure 12. Spin-density patterns computed for mono-reduced saddle-shaped distorted [**Ref5**]$^-$ (left) and mono-oxidized axially distorted [**Ref5**]$^+$ (right); contour value 5×10^{-4} a.u.

sic electronic polarization of dissymmetric pyrimidinyl connectors. Planarization occurs upon local enhancement of ASPs about P-B linkages whether resulting from intramolecular electron density displacement (that is, ICTs regardless of the direction) or promoted SD perturbation, which are both attached to ^{3}An* formation. Clearly, even though the electron-withdrawing properties of the pm connectors and dangling SCs are not very efficient in terms of net ICT, they do have a noticeable influence in these regards, facilitating the possibility of going through borderline P/B steric repulsion. The extent of the planarization is determined by local steric hindrance, and is driven to completion only in the case of regio-isomers *int*. Full achievement of planarization about the P-B linkage results in saddle-shaped distortion. The point is that small changes in the ground-state intramolecular parameters cause dramatically large electronic, magnetic, and structural changes in the lowest THEXI state.

The saddle-shaped structural relaxation in the lowest THEXI state: It is recognized that the resonance energy within polyacene is smaller for the central (inner) ring than for the outer rings.[65,66] In the case of anthracene, this is further supported by the well-documented particular reactivity associated with its central ring, and more especially to positions C9^{An} and C10^{An}.[67–69] The lowered "aromaticity" of the inner ring of polyacene is ascribed to so-called benzoannulation,[70] which also contributes to enhancing conformational flexibility of the acene backbone.[71] Appending bulky groups at positions C9^{An} and C10^{An} adds some structural constraints to the central ring of An by introducing steric repulsions with *peri* atoms of adjacent (outer) rings. Such decorations further contribute to the reduction of the stability of the molecule, making it more reactive. If the bulky substituent is isotropic (e.g., *t*Bu), structural relaxation involves the onset folding of the An backbone[44,72] that is, saddle-shaped distortion. If the bulky group displays anisotropic features (e.g., aryl plane), conformational change (e.g., canting of the plane of the substituent) may be sufficient to relax intramolecular constraints so as to maintain the planarity of the acene skeleton, as in the case of the presently investigated PMMDs (axially distorted in the GS). In some limiting cases, however, like in anthraquinodimethane motifs of π-extended quinones or TTF derivatives, the folding of the acene backbone is energetically less demanding than the alteration of the quinoid pattern involving the central ring (Figure 10), which is therefore considered as being no longer aromatic. Therefore, it is not surprising that, in some borderline cases where the steric congestion about the central ring of An is not so large (e.g., pm-derivative regio-isomers *int*. versus regio-isomers *ext*. or ph-based analogues), a change in the electronic features likely to reinforce the double-bond character of the P-B linkage (i.e., likely to favor locally the planar layout of the two-component system) can be sufficient to get around the reduced resonance energy of the central ring, eventually resulting in a structural folding of the acene (α_1 and α_2 in Figure 3; saddle-shaped distortion). Besides, enhanced benzoannulation can be visualized in Figure 7, in the case of **Td5***. For bifurcating PMMDs, that is, photoexcited regio-isomer *int*., the electronic perturbation is induced by light. Following photoinduced generation of the SD-perturbing triplet of anthracene (as a transient magnetic supersite[14]) and intramolecular charge redistribution (ICTs), the planarization occurs primarily, eventually resulting in the saddle-shaped structural relaxation of the LTS.

With respect to the possible participation of valence Dewar isomerization in the saddle-shaped distortion (cf. tetrafluoro-DMABN), it is interesting to note that parent [pm-An-pm] regio-isomer *int*. (**Ref5**) does not show Dewar features when saddle-shaped distortion results from one-electron reduction (Figure 12), whereas it does when photo-promoted in its triplet lowest THEXI state whether isolated (e.g., **Ref5***; Figure SVIII) or embedded within PMMDs (see for instance **HTd71***, Figure 8). Hence, one can reasonably infer that the onset Dewar bond formation is probably the consequence of the combination of: 1) the folding occurring about both the C9^{An} and C10^{An} positions (which then become closer in space: parameter *r* in Figure 3, Tables 1–3); with 2) the large ASPs usually located at these peculiar positions when anthracene is promoted in its triplet excited state.[14] In other words, the onset formation of the Dewar valence isomer within regio-isomers *int*. in their lowest THEXI state is not the driving force for the folding of the molecules but rather the consequence of it. Moreover, this assertion is consistent with the fact that deviation from planarity for the ground-state geometry of anthracene (bearing sterically-demanding substituents) is a prerequisite for photochemical valence isomerization. Indeed, 9,10-Dewar anthracene is not accessible by direct photochemical isomerization of bare anthracene.[69] It is also in line with previous issues regarding the origin of the bending of [B-P-B]*, namely the borderline steric encumbrance of the pyrimidinyl ring.

Unraveling planarization and saddle-shaped distortion: Beyond intricate intramolecular electronic effects and the proper orientation of pm connectors with respect to the An core (regio-isomerism), the suitable balance between conflicting local intercomponent (P/B) steric repulsion and propensity to planarize (θ_1*) is also mandatory to produce the saddle-shaped distortion in the excited state, and deserves to be further investigated. To this end, the excited-state be-

 © 2008 Wiley-VCH Verlag GmbH & Co. KGaA, Weinheim

haviors of pm-analogues (**Td3bis** and **Td4bis** regio-isomers *int.*, Figure 13) of the already described[14] ph-based **Td3** and **Td4** PMMDs (Figure 1) have been studied. Compared to

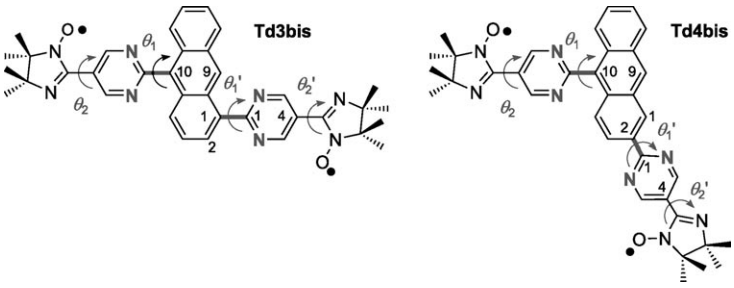

Figure 13. Disentangling planarization from saddle-shaped distortion. Labeling and numbering schemes of **Td3bis** and **Td4bis** model triads.

substitution at the $C10^{An}$ position (involving two critical H *peri*), [B-SC] extensions experience lower and decreased steric congestion about the P-B linkage on being connected at positions $C1^{An}$ (one H *peri* of the two is critical; **Td3bis**) and $C2^{An}$ (neither of the two H *peri* is critical; **Td4bis**), respectively (Figure 13).

Optimized structures of **Td3bis*** and **Td4bis*** show only partial saddle-shaped distortion (correlated with uncompleted planarization: $\theta_1^* \neq 0°$), essentially involving the branch connected at position $C10^{An}$, with $\theta_1^* = 21°$ and 25°, respectively (Supporting Information; Figure S IX).[73] Full planarization ($\theta_1'^* \approx 0°$) is, however, reached for the second branch connected at positions $C1^{An}$ and $C2^{An}$, and is accompanied by a slight folding of the acene skeleton in the former case, with no distortion at all found in the latter case (Figures 13 and S IX). For the ph-based analogues **Td3*** and **Td4***, this second branch was computed to remain canted with respect to the An platform despite significant planarization, with $\theta_1'^* \approx 45°$ and 29°, respectively.[14] This finding definitively validates the relevance of the present optimization strategy of the PMMDs, relying on the substitution of phenyl with pyrimidinyl as connectors *B*. Besides, J_{ES} values calculated with related dyad functional models **Dd3bis*** (connection at $C1^{An}$) and **Dd4bis*** (connection at $C2^{An}$) indeed provide greater coupling constants than for ph-based derivatives: +259 K (vs. +83 K for **Dd3***)[14] and +177 K (vs. +100 K for **Dd4***).[14] Since a full planarization of the branches connected at positions $C1^{An}$ and $C2^{An}$ is reached for **Td3bis*** and **Td4bis***, contrary to **Td3*** and **Td4***, the *J* values are ruled only by the larger ASP computed at position $C1^{An}$ and $C2^{An}$.

It is noteworthy that deviation from full planarization for the [B-SC] arm connected at $C10^{An}$ is much more pronounced within **Td3bis*** and **Td4bis*** than within the **Dd5*** parent molecule ($\theta_1^* = 11.6°$; Figure 4), indicating once again that there exists an interaction between the two extensions even though they are connected to different rings of An. Basically, this mutual influence can be ascribed to the electron-withdrawing properties of pyrimidine (assisted by dangling SCs when present), which contribute to the delocalization of the SD perturbations attached to both the $^3An^*$ and the SCs, thus lowering accordingly the critical ASP values about key P-B linkages. Owing to the intrinsic uneven distribution of SD over the acene backbone for An in its triplet state (larger ASPs are found at $C9^{An}/C10^{An}$ positions of the inner ring than at $C1^{An}+C2^{An}$ and related positions of the two outer rings),[14] the averaging effect of the local ASPs upon delocalization is more dramatic in **Td3bis*** and **Td4bis*** than in symmetric **Td5***. This difference is likely to explain the smaller amplitude of the saddle-shaped distortion about $C10^{An}$ (related to the smaller amplitude of the planarization) computed for both **Td3bis*** and **Td4bis*** compared to **Td5*** ($\theta_1^* \approx 0°$; Table 1).

General comments: The present work was essentially aimed at rationally improving the photomagnetic functioning of a class of PMMDs designed for photoinduced spin alignment[10] with a view to the future development of molecular spintronics devices.[14] To do so, the full analysis of structural and electronic features of molecular prototypes at the theoretical level was mandatory. This study also gave us the unique opportunity to gain some insights into the conditions under which functional emergences, here embodied by the saddle-shaped distortion, can be initiated by light.

Functional optimization of PMMD prototypes (molecular design): A great deal of effort has already been devoted to improving the working mode of the PMMD prototypes investigated in the present work. Hitherto, optimizations were essentially directed towards the quest for: 1) suitable P and SC functional components, and 2) connection scheme alternatives to usual $C9^{An}/C10^{An}$ substitution in the case of anthracene as the P element.[10a,c,h,14]

Regarding dual P/SC functional elements alternative to anthracene, there are the silole luminophore,[74,75] and pyrene,[10c,f] as well as metallo-porphyrins[76] or metallo-phtalocyanines,[77] and even corannulene[78] or fullerene[79] derivatives.

With respect to the selection of the SCs, they have to be π-conjugative (as is not the case for the popular TEMPO radical, for instance) because of the working mode of the PMMDs (Scheme 1), which relies on the use of superexchange pathways. Also, they should neither endanger the precious photophysical properties of P (e.g., quench the triplet state of An),[80,81] nor favor (including getting involved in) the resonant contribution of quinoid forms, as is potentially the case for the nitronyl-nitroxide (NN) radical. Thus, imino-nitroxyl (IN)[10d,i,j] and oxoverdazyl (OV)[10c,f,g] radicals have emerged as candidates of choice.

Much less attention has been paid to the connector units B. Besides meeting requirements attached to experimental methodology in some particular cases (such as the increase in the extent of the π-system to reduce *J* and make it possible to measure the hyperfine coupling constant a_N with EPR setup),[82] the intervening (phenyl) ring contributes: 1) as a stabilizer: to reinforce the stability of dangling radicals

 © 2008 Wiley-VCH Verlag GmbH & Co. KGaA, Weinheim

(SCs) by conjugation,[83] 2) as a connector: to ensure magnetic communication by propagating spin density perturbations (polarization),[84] also easing enhanced (selective) intersystem crossing (isc),[10h,85] 3) as a spacer: to diminish steric congestion about the immediate vicinity of the An core, especially when multiple connections are envisioned.[14] We have shown in the present work that some drawbacks related to intramolecular steric hindrance could be overcome by replacing the phenyl spacer with other heterocyclic moieties, such as 2-pyrimidinyl. It is worth noting that the B element may also be responsible for the deterioration of key photophysical features of P, as is potentially the case for remote SCs. For instance, tetrazine could not be used as the bridging element (B) in spite of its appealing structural and electron-withdrawing features, because of its low-lying triplet state ($\Delta E(T_1-S_0)=1.13$ eV)[86] computed to quench the triplet state of An (lying at 1.81 eV).[87]

All in all, the most promising composition up to now reported for the presently studied PMMD prototypes is comprised of: anthracene as the P component, 2-pyrimidine as the B component, and oxoverdazyl as the SC. The best topological connection scheme is when pm is linked to An at the $C9^{An}$ and $C10^{An}$ positions, moreover according to regio-isomerism "*int.*". The true substance of our molecular design reasoning, which led to the optimized PMMD **Td7**, is depicted schematically in Figure 14.

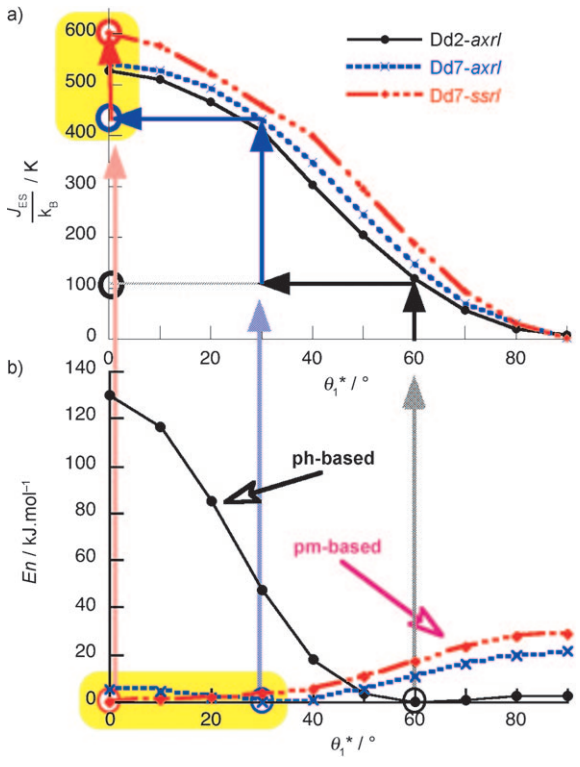

Figure 14. Intramolecular magneto-structural correlation in the lowest THEXI state (LTS) underlying the optimization approach of PMMDs (**Dd2-*axrl*/Dd7-*axrl*/Dd7-*ssrl***). *Axrl* and *ssrl* suffixes refer to types of distortion: *axially* and *saddle-shaped*, respectively (see text). From bottom to top: correspondence between b) θ_1* angles and a) J_{ES} values. Emerging behavior is highlighted in yellow.[88]

Structural constraints have been imposed on **Dd7** to force its LTS to relax according to the sole axially distorted pathway (**Dd7-*axrl***) in Figure 14). Thus, only planarization[38] about the P-(θ_1)-B intercomponent linkages is allowed (θ_2*=0°), as in the case of **Dd2** phenyl-based PMMD (denoted **Dd2-*axrl*** in Figure 14). In the case of **Dd7-*ssrl***, the supplementary folding distortion (Figures 3 and 5) attached to the onset formation of the saddle-shaped conformation is allowed for **Dd7**. For all three structures, the energy variation has been assessed as a function of the θ_1* (angular increment: 10°; Figure 14, bottom). Looking at the three plots, it clearly appears that ph-based and pm-based PMMDs behave differently. Besides shifting the minimum value of θ_1* towards 0°, replacement of phenyl with 2-pyrimidinyl as the connector also significantly lowers the rotational energy barrier, as evidenced by the overall shape of the potential energy surfaces (PES), which become much flatter for **Dd7-*axrl*** and **Dd7-*ssrl*** (Figure 14; bottom part). "Equilibrium geometries" (energy minima) of LTS are found at $\approx\theta_1$*=60°, 30°, and 0° for **Dd2-*axrl***, **Dd7-*axrl***, and **Dd7-*ssrl***, respectively. For each of the incremental geometries of the three structures, the J_{ES}/k_B value has also been calculated[88] (Figure 14; top). The three curves have roughly the same sinusoidal profile, lying close to one another regardless of the nature of the connector. The small impact of the electron-withdrawing ability of pm (compared to ph) on the J_{ES} values is visualized by the slight increase of J_{ES} at each θ_1* value (below 80°) computed on going from **Dd2-*axrl*** to **Dd7-*axrl*** and **Dd7-*ssrl***. The most spectacular effect of the pyrimidinyl substitution over exchange couplings in the LTS is obviously attached to the dramatic change of the θ_1* values. At this stage, it is worth distinguishing between two types of improvements. On the one hand, there is the *expected* change represented by the behavior of **Dd7-*axrl***, leading to θ_1* ≈30° and J_{ES}/k_B ≈400 K, a value well above previously reported characteristics of ph-based PMMDs (J_{ES} is increased by a factor of two).[14] On the other hand, there is the *unexpected* improvement associated with the emerging behavior represented by **Dd7-*ssrl*** and characterized by the light-induced saddle-shaped distortion of the lowest THEXI state. This emergence gives rise to a further increase of the J_{ES} value of 50% up to ≈600 K, which is actually the optimum (possible) magnetic coupling for this kind of PMMD prototype (Figure 14). Another striking point is that this substantial increase of J_{ES} (from 400 to 600 K) is, however, related to a fairly small gain in energy (≈−3 kcal mol^{-1}). This is a supplementary appearance of the extreme sensitivity of the emergent behavior.

From an experimental viewpoint, synthesis of the most promising prototypes regio-isomers *int.* is currently underway. Interestingly, the fact that J_{ES}/k_B amounts to at least 400 K, regardless of the intervening saddle-shaped distortion, should allow us to detect the lowest photoexcited high-spin state by time-resolved electron spin resonance (TR-ESR) experiments.[10] The large J_{ES} value does not directly permit, by itself, the selective detection of the high-spin state, because the TR-ESR experiment detects the non-equi-

 © 2008 Wiley-VCH Verlag GmbH & Co. KGaA, Weinheim

librium state before thermal equilibrium. However, if there is any spin-orbit mediated mechanism connecting the lowest high-spin state and other upper-lying spin states, a rapid relaxation will occur towards the lowest high-spin excited state. As a matter of fact, in our previous work on phenylanthracene radical systems (Figure 1),[10] selective detection of the lowest high-spin state was realized for all the cases of large positive J_{ES} values. Actually, even in the case of *m,p*-isomers[10a] showing very small J_{ES} values, both quintet and triplet states were simultaneously observed.[10a] Therefore, we can safely expect to detect selectively the lowest high-spin states of the presently investigated regio-isomers. Even at room temperature and in fluid solution, in which excited-state structural change should not be impeded for the regio-isomers *int.*, and on the basis of the robust intramolecular spin alignment, the selective detection of the lowest high-spin state is expected at both non-equilibrium and thermal equilibrium states. On the other hand, photophysical study of various PMMDs, including the highly luminescent **Ref5** and **Ref6** reference species, should allow us to gain further insights into both the nature and the magnitude of hypothesized photoinduced ICTs.

Light-induced functional emergence at the intramolecular level; identified pattern: Upon light excitation, certain molecules can become entirely different either at the level of their electronic and structural features, up to becoming genuine new, and sometimes unexpected, species in the excited state. It is typical among these highly light-sensitive molecular systems (whose photo-triggered behavior can be merely unpredictable) that the transient phenomena we refer to as light-induced functional emergences (LIFE)[8b] may occur. Photoinduced symmetry breaking (PISB), the "sudden polarization" effect,[89] and excited-state mixed-valence distortions[90] can be viewed as illustrations of such singular behaviors. For instance, symmetric chromophoric species like tetraphenylethylene, 9,9′-bifluorenylidene[50] and the recently reported cofacial homo-dimer of perylenediimide,[91] achieve a kind of "functional disproportionation" upon photon absorption.[5492]

Even though functional emergences can happen in apparently quite simple systems,[93] as illustrated above, the probability for them to occur increases with the system's complexity.[94,95] In this context, it is noteworthy that there is currently a marked propensity for advanced PMDs to become ever more complex while intending multifunctional integration. Then, the problem of (functional) emergences[96,97] within these PMDs is raised since emergences basically occur to the detriment of (multifunctional) integration, which fits in a reductionist scheme.[94] It is therefore of paramount importance to clarify the conditions under which bifurcating behaviors of PMDs are most likely to be favored,[98] as they may render null the design strategies based on the conceptual corpus of supramolecular photochemistry.[2,3,5,99]

Extreme sensitivity to the variation of molecular parameters (sometimes also including exogenous factors)[100] is one of the hallmarks of emergences. In the present case, occurrence of structural distortion is a matter of balance between intramolecular factors, namely steric repulsion and electronic stabilization. In closely coupled systems with a critical combination of components, such a balance may change on going from the GS to the ES. This is the case here. Upon replacing the phenyl connectors with pyrimidinyl ones having their nitrogen atoms pointing towards the anthracene core (regio-isomer *int.*), steric repulsion is significantly decreased. This situation translates into a flattened PES (Figure 14) which, in its turn, accounts for the extreme sensitivity of the molecules to slight intramolecular changes (mostly of electronic nature). Typically, the GS geometry of pm-based PMMDs (*int.*) is found to be flatter than that of ph-based analogues (Figure 14), even though coplanarity is not reached ($\theta_1 \neq 0$). The balance remains in favor of steric repulsion. Upon light excitation, the electron-spin density distribution is significantly changed (marked polarization) and to a lesser extent, there is also a charge redistribution (slight ICT), with the result that the balance turns to be in favor of electronic stabilization correlated with planarization about θ_1: the exocyclic bonds get shorter on gaining partial double bond character. In this case, steric repulsion is overcome by the saddle-shaped distortion of the whole molecule, including the anthracene platform.

Beyond the proper structural features, this bifurcating behavior is clearly related to multi-functional intermingling and resulting intramolecular intricacy. Anthracene is primarily the photosensitizer (P), but is also a coupling element, an exciton provider (transient spin carrier) and an electron donor. Pyrimidines are primarily connectors (B), but are also electron donors or acceptors (eventually assisted by the dangling SCs). Stable radicals are primarily the (persistent) spin carriers (SC), but are also key sources of disruption for spin density and electron acceptors.

B not only mediates the magnetic coupling by supporting spin polarization, but also actively contributes to undergoing ICT of importance to pass the threshold of full planarization leading to saddle-shaped distortion. Of interest, also, is the tuning of the excited-state redox reactivity (electron donor/acceptor) of ambivalent anthracene by the regio-isomerism associated with the appended pyrimidinyl substituents within [pm-An-pm] assemblies lacking the SCs (**Ref5** and **Ref6**). Regarding the SCs, although apparently not strictly necessary, saddle-shaped distortion is assisted by their presence through their SD perturbing and weak electron-accepting activities. Although there is no doubt concerning the origin of the saddle-shaped distortion, experiment is necessary to assess to what extent the presence of the SC(s) is mandatory to fully develop the peculiar structural distortion.

Brought together, all these issues allow us to present the promising pattern of the novel molecular assembly depicted schematically in Figure 15.

The emerging motif is comprised of 9,10-dipyrimidinyl-anthracene (regio-isomer *int.*), most likely transposable to other polyacene (pAc) derivatives (i.e., pm-pAc-pm), and of

 © 2008 Wiley-VCH Verlag GmbH & Co. KGaA, Weinheim

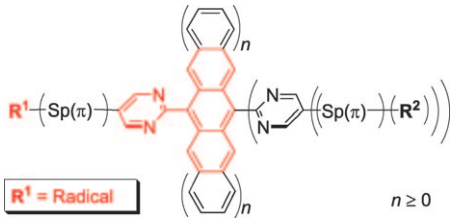

Figure 15. Emerging pattern (in red) supporting new light-triggered functional schemes. Sp(π) is a π-conjugative spacer.

a properly linked radical source (Figure 15). On the bases of its intriguing intrinsic features unveiled in the present work, including the photo-switching of the preferential axis for π-delocalization within the cruciform assembly (cf. Figure 9), this molecular pattern is expected to give rise to light-driven functional schemes still to be explored, which are closely attached to appealing saddle-shaped distortion in photoexcited state(s). In addition to forthcoming developments in photomagnetism (including molecular spintronics),[10c,14,101] one may envision the implementation of the identified molecular motif (with proper decorations) in the following fields:[16] 1) molecular photonics: nonlinear optics including reverse saturable absorption properties; 2) molecular electronics: photo-switchable molecular wire (for controlled electron transfer; cf. Figure 9); 3) nano-mechanics (molecular machines and muscles): taking advantage of the change of the molecular shape (including edge-to-edge distance, see ref. [48]) to design light-triggered molecular actuators[102] and photo-contractile molecule-based materials; 4) solar energy conversion and storage: driving photosensitized Dewar valence isomerization to completion, to store light energy in the form of chemical constraint (as in the case of the norbornadiene/quadricyclane couple).[103]

Conclusion

Conclusions concerning photoinduced spin alignment within prototypes photomagnetic molecular devices (PMMDs) are twofold as they deal with both the improved photomagnetic behavior of PMMDs on the one hand, and possible excited-state bifurcating behavior of some of these PMMDs on the other hand.

Firstly, in the field of molecular photomagnetism, towards molecular spintronics,[14] the type of PMMDs herein investigated has been greatly improved. Even without the saddle-shaped distortion, improvement of J_{ES} is sufficient to make PMMDs operative at room temperature ($J_{ES}/k_B > +400$ K).[104] This is a step towards the implementation of molecular spintronic devices. Increasing the number of [B-SC] branches (extensions) about P[14] as well as managing to obtain $J_{GS} = 0$ and $|J_{ES}| \gg 0$, and even: $J_{GS1} = 0$ and $|J_{GS2}| \gg 0$ in the limiting case of a light-driven bistable system (ΔE-(LTS-GS)$\rightarrow$0), are among the following steps.[16] Last, it is worth noting that, when photo-promoted in its paramagnetic lowest excited state, central P* behaves as a nexus with respect to the dangling radicals.[14] Therefore, branched architectures derived from present PMMD prototypes are a promising alternative to strategies relying on particular π-topologies[105] (including cross-conjugation) and spin-dependent delocalization in exchange couplings[106] to design new (photo-switchable) high-spin molecules.[14,107]

Secondly, we have theoretically investigated a series of molecular systems, all affiliated in the ground state. Among them, regio-isomers *int.* were found to show bifurcating behavior when photo-promoted in their lowest THEXI state. At the electronic level, these singular species are rightly referred to as large (excited) molecules versus supramolecular (excited) species for the others. Here, we face a phenomenon we refer to as a light-induced functional emergence (LIFE). Out of this complexity, the intriguing behavior of 9,10-dipyrimidinyl-anthracene (regio-isomer *int.*), especially when properly associated with a radical, has been identified. This molecular pattern is predicted to undergo a saddle-shaped distortion (upon light excitation) that is of potential interest in various research fields relying on photoactive functional molecules. Beyond the particular features attached to this pattern (including a proper balance between structural and electronic effects), the impact of an intramolecular radical source has been highlighted and radicals are therefore identified as key ingredients for forthcoming works devoted to the further embodiment of light-induced functional emergences and for the search of emergences at the intramolecular level in general. In so doing, we are gaining some insights into the boundaries of multifunctional integration at the intramolecular level within closely coupled systems.

Acknowledgements

The IDRIS (French national computer center) is gratefully acknowledged for computer time allocation within the Project 07183. P.P.L., I.C. and C.A. are grateful to the French National Agency for Research (ANR) "programme blanc" (NEXUS project; No. BLAN07-1-196405) as well as to European Egide integrated action program "Germaine de Staël" (PAI-10612NL) for financial support. P.P.L. is also indebted to the French ministry of research for funding (ACI project No. JC4123). Y.T. is grateful to the Grant-in-Aid for Scientific Research on General Research (B) (No. 13440211) from JSPS and to the Grant for Scientific Research on Priority Areas "Molecular Theory for Real Systems" (Area No. 461, Proposal No. 19029039) from MEXT, Japan.

[1] Selected recent references: a) D. Gust, T. A. Moore, A. L. Moore, *Chem. Commun.* **2006**, *11*, 1169–1178, and references therein; b) V. Balzani, *Photochem. Photobiol. Sci.* **2003**, *2*, 459–476, and references therein; c) S. Saha, J. F. Stoddart, *Chem. Soc. Rev.* **2007**, *36*, 77–92, and references therein; d) M. R. Wasielewski, *J. Org. Chem.* **2006**, *71*, 5051–5066, and references therein.

[2] V. Balzani, L. Moggi, F. Scandola in *Supramolecular Photochemistry*, (Eds.: V. Balzani, D. Reidel) Publishing Co., Dordrecht, The Netherlands, **1987**, pp. 1–28.

[3] a) V. Balzani, *Tetrahedron* **1992**, *48*, 10443–10514; b) V. Balzani, F. Scandola, *Supramolecular Photochemistry*, Ellis Horwood, Chichester, U.K., **1991**; Chapter 12.

 © 2008 Wiley-VCH Verlag GmbH & Co. KGaA, Weinheim

[4] a) J.-M. Lehn, *Angew. Chem.* **1988**, *100*, 91–116; *Angew. Chem. Int. Ed. Engl.* **1988**, *27*, 89–112; b) J.-M. Lehn, *Angew. Chem.* **1990**, *102*, 1347–1362; *Angew. Chem. Int. Ed. Engl.* **1990**, *29*, 1304–1319.
[5] V. Balzani, L. De Cola, L. Prodi, F. Scandola, *Pure Appl. Chem.* **1990**, *62*, 1457–1466.
[6] J.-P. Sauvage, J.-P. Collin, J.-C. Chambron, S. Guillerez, C. Coudret, V. Balzani, F. Barigelleti, L. De Cola, L. Flamigni, *Chem. Rev.* **1994**, *94*, 993–1019.
[7] P. P. Lainé, I. Ciofini, P. Ochsenbein, E. Amouyal, C. Adamo, F. Bedioui, *Chem. Eur. J.* **2005**, *11*, 3711–3727.
[8] a) P. P. Lainé, F. Bedioui, F. Loiseau, C. Chiorboli, S. Campagna, *J. Am. Chem. Soc.* **2006**, *128*, 7510–7521; b) P. P. Lainé, F. Loiseau, S. Campagna, I. Ciofini, C. Adamo, *Inorg. Chem.* **2006**, *45*, 5538–5551; c) I. Ciofini, P. P. Lainé, F. Bedioui, C. Adamo, *J. Am. Chem. Soc.* **2004**, *126*, 10763–10777; d) P. Lainé, F. Bedioui, E. Amouyal, V. Albin, F. Berruyer-Penaud, *Chem. Eur. J.* **2002**, *8*, 3162–3176; e) P. Lainé, F. Bedioui, P. Ochsenbein, V. Marvaud, M. Bonin, E. Amouyal, *J. Am. Chem. Soc.* **2002**, *124*, 1364–1377; f) P. Lainé, E. Amouyal, *Chem. Commun.* **1999**, 935–936.
[9] P. P. Lainé, S. Campagna, F. Loiseau, *Coord. Chem. Rev.* **2008**, *252*, 2552–2571.
[10] a) Y. Teki, T. Toichi, S. Nakajima, *Chem. Eur. J.* **2006**, *12*, 2329–2336; b) T. Toichi, Y. Teki, *Polyhedron* **2005**, *24*, 2337–2340; c) Y. Teki, *Polyhedron* **2005**, *24*, 2299–2308; d) Y. Teki, *Polyhedron* **2005**, *24*, 2185–2188; e) Y. Teki, S. Nakajima, *Chem. Lett.* **2004**, *33*, 1500–1501; f) Y. Teki, M. Kimura, S. Narimatsu, K. Ohara, K. Mukai, *Bull. Chem. Soc. Jpn.* **2004**, *77*, 95–99; g) Y. Teki, M. Nakatsuji, Y. Miura, *Mol. Phys.* **2002**, *100*, 1385–1394; h) Y. Teki, S. Miyamoto, M. Nakatsuji, Y. Miura, *J. Am. Chem. Soc.* **2001**, *123*, 294–305; i) Y. Teki, *Polyhedron* **2001**, *20*, 1163–1168; j) Y. Teki, S. Miyamoto, K. Iimura, M. Nakatsuji, Y. Miura, *J. Am. Chem. Soc.* **2000**, *122*, 984–985.
[11] a) Y. Teki, H. Tamekumi, K. Haruta, J. Takeuchi, Y. Miura, *J. Mater. Chem.* **2008**, *18*, 381–391; b) Y. Teki, H. Tamekumi, J. Takeuchi, Y. Miura, *Angew. Chem.* **2006**, *118*, 4782–4786; *Angew. Chem. Int. Ed.* **2006**, *45*, 4666–4670.
[12] M. Konstantaki, E. Koudoumas, S. Couris, P. Lainé, E. Amouyal, S. Leach, *J. Phys. Chem. B* **2001**, *105*, 10797–10804.
[13] P. Lainé, V. Marvaud, A. Gourdon, J.-P. Launay, R. Argazzi, C.-A. Bignozzi, *Inorg. Chem.* **1996**, *35*, 711–714.
[14] I. Ciofini, P. P. Lainé, M. Zamboni, C. A. Daul, V. Marvaud, C. Adamo, *Chem. Eur. J.* **2007**, *13*, 5360–5377.
[15] This is for instance the case of nexus states as active components of molecular spintronics devices (see ref [14]) or the case of toroïdal delocalization within molecular dendritic connectors: see a) C. Lambert, *Angew. Chem.* **2005**, *117*, 7503–7505; *Angew. Chem. Int. Ed.* **2005**, *44*, 7337–7339, and references therein; b) I. Ciofini, P. P. Lainé, C. Adamo, *Chem. Phys. Lett.* **2007**, *435*, 171–175.
[16] Work in progress.
[17] N. J. Turro, J. K. Barton, *J. Biol. Inorg. Chem.* **1998**, *3*, 201–209.
[18] L. Bogani, W. Wernsdorfer, *Nat. Mater.* **2008**, *7*, 179–186.
[19] Q. Mi, E. T. Chernick, D. W. McCamant, E. A. Weiss, M. A. Ratner, M. R. Wasielewski, *J. Phys. Chem. A* **2006**, *110*, 7323–7333.
[20] Note that in IUPAC nomenclature the use of aminoxyl instead of nitroxyl is recommended.
[21] a) R. Passalacqua, F. Loiseau, S. Campagna, Y.-Q. Fang, G. S. Hanan, *Angew. Chem.* **2003**, *115*, 1646–1649; *Angew. Chem. Int. Ed.* **2003**, *42*, 1608–1611; b) Y.-Q. Fang, N. J. Taylor, G. S. Hanan, F. Loiseau, R. Passalacqua, S. Campagna, H. Nierengarten, A. Van Dorsselaer, *J. Am. Chem. Soc.* **2002**, *124*, 7912–7913.
[22] From the viewpoint of methodology, it is worth studying a series of affiliated candidates rather than individual species so as to rely on trends to limit misleading issues.
[23] Gaussian Development Version, Revision B.05, M. J. Frisch, G. W. Trucks, H. B. Schlegel, G. E. Scuseria, M. A. Robb, J. R. Cheeseman, J. A. Montgomery, Jr., T. Vreven, K. N. Kudin, J. C. Burant, J. M. Millam, S. S. Iyengar, J. Tomasi, V. Barone, B. Mennucci, M. Cossi, G. Scalmani, N. Rega, G. A. Petersson, H. Nakatsuji, M. Hada, M. Ehara, K. Toyota, R. Fukuda, J. Hasegawa, M. Ishida, T. Nakajima, Y. Honda, O. Kitao, H. Nakai, X. Li, J. E. Knox, H. P. Hratchian, J. B. Cross, C. Adamo, J. Jaramillo, R. Gomperts, R. E. Stratmann, R. Cammi, C. Pomelli, J. Ochterski, P. Y. Ayala, K. Morokuma, W. L. Hase, P. Salvador, J. J. Dannenberg, V. G. Zakrzewski, S. Dapprich, A. D. Daniels, M. C. Strain, O. Farkas, D. K. Malick, A. D. Rabuck, K. Raghavachari, J. B. Foresman, J. V. Ortiz, Q. Cui, A. G. Baboul, S. Clifford, J. Cioslowski, B. B. Stefanov, G. Liu, A. Liashenko, P. Piskorz, I. Komaromi, R. L. Martin, D. J. Fox, T. Keith, M. A. Al-Laham, C. Y. Peng, A. Nanayakkara, M. Challacombe, P. M. W. Gill, B. Johnson, W. Chen, M. W. Wong, C. Gonzalez, and J. A. Pople, Gaussian, Pittsburgh PA, **2003**.
[24] C. Adamo, V. Barone, *J. Chem. Phys.* **1999**, *110*, 6158–6170.
[25] J. P. Perdew, K. Burke, M. Ernzerhof, *Phys. Rev. Lett.* **1996**, *77*, 3865–3868.
[26] T. H. Dunning Jr., P. J. Hay, In *Modern Theoretical Chemistry*; H. F., Schaefer III, Ed.; Plenum: New York, 1976, pp.1–28.
[27] W. J. Hehre, R. Ditchfield, J. A. Pople, *J. Chem. Phys.* **1972**, *56*, 2257–2261.
[28] W. Heisenberg, *Z. Phys.* **1928**, *49*, 619–636.
[29] P. A. M. Dirac, *Proc. R. Soc. London Ser. A* **1929**, *123*, 714–733.
[30] J. H. Van Vleck, *The Theory of Electric and Magnetic Susceptibilities*, Oxford University Press, New-York, **1932**.
[31] a) L. Noodleman, J. G. Norman, *J. Chem. Phys.* **1979**, *70*, 4903–4906; b) L. Noodleman, *J. Chem. Phys.* **1981**, *74*, 5737–5743; c) J. G. Norman, P. B. Ryan, L. Noodleman, *J. Am. Chem. Soc.* **1980**, *102*, 4279–4282.
[32] K. Yamaguchi, F. Jensen, A. Dorigo, K. N. Houk, *Chem. Phys. Lett.* **1988**, *149*, 537–542.
[33] A. A. Ovchinnikov, J. K. Labanowski, *Phys. Rev. A* **1996**, 53, 3946–3952.
[34] I. Ciofini, C. A. Daul, *Coord. Chem. Rev.* **2003**, *238–239*, 187–209.
[35] I. Ciofini, C. Adamo, V. Barone, G. Berthier, A. Rassat, *Chem. Phys.* **2005**, *309*, 133–141.
[36] M. Cotlet, S. Masuo, G. Luo, J. Hofkens, M. van der Auweraer, J. Verhoeven, K. Müllen, X. S. Xie, F. De Schryver, *Proc. Natl. Acad. Sci. USA* **2004**, *101*, 14343–14348.
[37] R. Ziessel, G. Ulrich, R. C. Lawson, L. Echegoyen, *J. Mater. Chem.* **1999**, *9*, 1435–1448.
[38] The term *planarization* specifically refers to the molecular *structural relaxation* towards planarity occurring on going from the ground state to the lowest THEXI state.
[39] a) A. S. Batsanov, M. R. Bryce, M. A. Coffin, A. Green, R. E. Hester, J. A. K. Howard, I. K. Lednev, N. Martín, A. J. Moore, J. N. Moore, E. Ortí, L. Sánchez, M. Savirón, P. M. Viruela, R. Viruela, T.-Q. Ye, *Chem. Eur. J.* **1998**, *4*, 2580–2592; b) M. R. Bryce, A. J. Moore, M. Hasan, G. J. Ashwell, A. T. Fraser, W. Clegg, M. B. Hursthouse, A. I. Karaulov, *Angew. Chem.* **1990**, *102*, 1493–1495; *Angew. Chem. Int. Ed. Engl.* **1990**, *29*, 1450–1452; c) M. R. Bryce, M. A. Coffin, M. B. Hursthouse, A. I. Karaulov, K. Müllen, H. Scheich, *Tetrahedron Lett.* **1991**, *32*, 6029–6032.
[40] M. Bendikov, F. Wudl, D. F. Perepichka, *Chem. Rev.* **2004**, *104*, 4891–4945, and references therein.
[41] a) U. Schubert, S. Hünig, A. Aumüller, *Liebigs Ann. Chem.* **1985**, 1216–1222; b) C. Kabuto, Y. Fukazawa, T. Suzuki, Y. Yamashita, T. Miyashi, T. Mukai, *Tetrahedron Lett.* **1986**, *27*, 925–928; c) N. E. Heimer, D. L. Mattern, *J. Am. Chem. Soc.* **1993**, *115*, 2217–2220.
[42] R. Gomez, C. Seoane, J. L. Segura, *Chem. Soc. Rev.* **2007**, *36*, 1305–1322, and references therein.
[43] H. Kurata, T. Tanaka, M. Oda, *Chem. Lett.* **1999**, 749–750.
[44] S. Grimme, S. D. Peyerimhoff, *J. Phys. Chem.* **1994**, *98*, 12927–12932.
[45] The dependence of the magnitude of an exchange coupling constant *J* to ASP has already been discussed in the literature. For the intermolecular case, see for instance H. M. McConnell, *J. Chem. Phys.* **1963**, *39*, 1910. For the intramolecular case, see for instance: a) Y. Teki, T. Takui, K. Sato, A. Yamashita, M. Okamoto, T. Kinoshita, K. Itoh, *Mol. Cryst. Liq. Cryst.* **1993**, *232*, 261–270; b) Y. Teki, K. Itoh in *Molecule-Based Magnetic Materials*, (Eds.: M. M.

 © 2008 Wiley-VCH Verlag GmbH & Co. KGaA, Weinheim

Turnbull, T. Sugimoto, L. K. Thompson) American Chemical Society, Washington, DC, **1996**, ACS Symposium Series 644, pp. 16–29; c) Y. Teki, K. Itoh in *Magnetic Properties of Organic Materials*, (Ed.: P. M. Lahti) Marcel–Dekker: New-York, **1999**, pp. 237–265, and references therein. The derivations of the formulas were based on the Hubbard model or HDVV Hamiltonian (not ab initio MO theory).

[46] This feature reveals the enhancement of benzoannulation within saddle-shaped distorted photoexcited triads.

[47] It is worth noting that in the case of axially distorted regio-isomers *ext.*, ΔE is virtually the same regardless of whether singly-branched dyads or doubly-branched triads are considered.

[48] The spatial expanse of the resonant pseudo-quinoid pattern, which essentially develops about the central part of the molecules, is not sufficient to involve remote SCs and pair their spins. The only additional antiferromagnetic contribution attached to the saddle-shaped distortion is at first glance related to enhanced through-space polarization interaction of remote SCs within triads. Indeed, structure optimization indicates that the edge-to-edge distance is shortened by ≈10–15% in the saddle-shaped conformation with respect to the axially distorted one (for instance, the distance between oxygen termini is reduced from 22.22 to 19.20 Å in the typical case of **Td7***). But this contaminating antiferromagnetic contribution is negligible anyway.

[49] This averaging of the ASPs upon delocalization is somewhat reminiscent of the averaging of structural distortions attached to excited-state electron delocalization over a large π-delocalized system: G. F. Strouse, J. R. Schoonover, R. Duesing, S. Boyde, W. E. Jones, Jr., T. J. Meyer, *Inorg. Chem.* **1995**, *34*, 473–487.

[50] Z. R. Grabowski, K. Rotkiewicz, W. Rettig, *Chem. Rev.* **2003**, *103*, 3899–4031, and references therein.

[51] S. Murali, V. Kharlanov, W. Rettig, A. I. Tolmachev, A. V. Kropachev, *J. Phys. Chem. A* **2005**, *109*, 6420–6429.

[52] N. Martín, L. Sánchez, C. Seoane, E. Ortí, P. M. Viruela, R. Viruela, *J. Org. Chem.* **1998**, *63*, 1268–1279.

[53] W. E. Jones, M. A. Fox, *J. Phys. Chem.J. Phys. Chem. A* **1994**, *98*, 5095–5099.

[54] In the case of bianthryl, that is, 9,9′-bianthracene, the two neutral photosensitizing anthracene moieties in the ground state concertively behave as a dyad comprised of an electron acceptor (A) and an electron donor (D) in the excited state, giving rise to a transient D^+–A^- (that is, An^+–An^-) redox pair, moreover correlated with a huge structural rearrangement, see ref [50].

[55] C. L. Barr, P. A. Chase, R. G. Hicks, M. T. Lemaire, C. L. Stevens, *J. Org. Chem.* **1999**, *64*, 8893–8897.

[56] J. B. Gilroy, S. D. J. McKinnon, B. D. Koivisto, R. G. Hicks, *Org. Lett.* **2007**, *9*, 4837–4840.

[57] R. M. Fico Jr. , M. F. Hay, S. Reese, S. Hammond, E. Lambert, M. A. Fox, *J. Org. Chem.* **1999**, *64*, 9386–9392.

[58] a) M. Tanaka, K. Matsuda, T. Itoh, H. Iwamura, *J. Am. Chem. Soc.* **1998**, *120*, 7168–7173; b) E. Coronado, C. Giménez-Saiz, M. Nicolas, F. M. Romero, E. Rusanov, H. Stoeckli-Evans, *New J. Chem.* **2003**, *27*, 490–497.

[59] A. Credi, V. Balzani, S. Campagna, G. S. Hanan, C. R. Arana, J.-M. Lehn, *Chem. Phys. Lett.* **1995**, *243*, 102–107.

[60] Aware of the possible bias of discussing absolute values of Mulliken charges as well as for clarity and consistency with ASP (that is, to avoid other charge analysis), we comment only on their variation on passing from the ground state to the LTS.

[61] M. S. Davis, K. Morokuma, R. W. Kreilick, *J. Am. Chem. Soc.* **1972**, *94*, 5588–5592.

[62] V. V. Pavlishchuk, A. W. Addison, *Inorg. Chim. Acta* **2000**, *298*, 97–102.

[63] By the yardstick of the diagnostic reduction degree of dangling SCs, it appears that the behavior of **HTd72** is more closely related to that of dyad species while the behavior of **HTd71** is rather akin to that of triads. These parentages are in line with issues previously derived from structural, magnetic, and electronic analyses.

[64] The relaxed axially distorted conformation of mono-reduced $[\mathbf{Ref5}]^-$ lies 0.08 eV above the saddle-shaped one, with $\theta_1 = 39.2°$ versus 23.1° for the folded conformation. Regarding the reduced reference regio-isomer *ext.*, that is $[\mathbf{Ref6}]^-$, the axially distorted conformation is by far the most stable conformation by at least 0.47 eV (Figure SVI). Note that both of the one-electron oxidized **Ref5** and **Ref6** species remain axially distorted (Figure SVII in the Supporting Information).

[65] a) P. Bultinck, R. Ponec, R. Carbo-Dorca, *J. Comput. Chem.* **2007**, *28*, 152–160; b) P. Bultinck, M. Rafat, R. Ponec, B. Van Gheluwe, R. Carbo-Dorca, P. Popelier, *J. Phys. Chem. A* **2006**, *110*, 7642–7648.

[66] a) J.-I. Aihara, *J. Am. Chem. Soc.* **2006**, *128*, 2873–2879; b) J.-I. Aihara, *J. Phys. Chem. A* **2005**, *109*, 3717–3721.

[67] a) A. R. Reddy, G. Fridman-Marueli, M. Bendikov, *J. Org. Chem.* **2007**, *72*, 51–61; b) J.-I. Aihara, *Phys. Chem. Chem. Phys.* **1999**, *1*, 3193–3197.

[68] H. Bouas-Laurent, A. Castellan, J.-P. Desvergne, R. Lapouyade, *Chem. Soc. Rev.* **2000**, *29*, 43–55.

[69] H.-D. Becker, *Chem. Rev.* **1993**, *93*, 145–172.

[70] R. Andreu, M. J. Blesa, L. Carrasquer, J. Garin, J. Orduna, B. Villacampa, R. Alcala, J. Casado, M. C. Ruiz Delgado, J. T. Lopez Navarrete, M. Allain, *J. Am. Chem. Soc.* **2005**, *127*, 8835–8845.

[71] O. V. Shishkin, A. Y. Kovalevskii, *J. Struct. Chem.* **2001**, *42*, 550–554.

[72] R. A. Pascal, Jr., *Chem. Rev.* **2006**, 106, 4809–4819.

[73] Notice that neither the SD pattern attached to **Td3bis*** nor that corresponding to **Td4bis*** display Dewar features, as expected (Figure SX in the Supporting Information).

[74] N. Roques, P. Gerbier, Y. Teki, S. Choua, P. Lesniakovà, J.-P. Sutter, P. Guionneau, C. Guérin, *New J. Chem.* **2006**, *30*, 1319–1326.

[75] a) N. Roques, P. Gerbier, U. Schatzschneider, J.-P. Sutter, P. Guionneau, J. Vidal-Gancedo, J. Veciana, E. Rentschler, C. Guérin, *Chem. Eur. J.* **2006**, *12*, 5547–5562; b) N. Roques, P. Gerbier, S. Nakajima, Y. Teki, C. Guérin, *J. Phys. Chem. Solids* **2004**, *65*, 759–762.

[76] a) K. Ishii, J. Fujisawa, A. Adachi, S. Yamauchi, N. Kobayashi, *J. Am. Chem. Soc.* **1998**, *120*, 3152–3158; b) K. Ishii, J. Fujisawa, Y. Ohba, S. Yamauchi, *J. Am. Chem. Soc.* **1996**, *118*, 13079–13080.

[77] K. Ishii, T. Ishizaki, N. Kobayashi, *J. Phys. Chem. A* **1999**, *103*, 6060–6062.

[78] S. Nishida, Y. Morita, T. Kobayashi, K. Fukui, A. Ueda, K. Sato, D. Shiomi, T. Takui, K. Nakasuji, *Polyhedron* **2005**, *24*, 2200–2204.

[79] a) L. Franco, M. Mazzoni, C. Corvaja, V. P. Gubskaya, L. Sh. Berezhnaya, I. A. Nuretdinov, *Chem. Commun.* **2005**, 2128–2130; b) F. Conti, C. Corvaja, A. Toffoletti, N. Mizuochi, Y. Ohba, S. Yamauchi, M. Maggini, *J. Phys. Chem. A* **2000**, *104*, 4962–4967; c) N. Mizuochi, Y. Ohba, S. Yamauchi, *J. Phys. Chem. A* **1999**, *103*, 7749–7750; d) N. Mizuochi, Y. Ohba, S. Yamauchi, *J. Phys. Chem. A* **1997**, *101*, 5966–5968; e) C. Corvaja, M. Maggini, M. Prato, G. Scorrano, M. Venzin, *J. Am. Chem. Soc.* **1995**, *117*, 8857–8858.

[80] N. Tanifuji, K. Matsuda, M. Irie, *Org. Lett.* **2005**, *7*, 3777–3780.

[81] N. Tanifuji, M. Irie, K. Matsuda, *J. Am. Chem. Soc.* **2005**, *127*, 13344–13353.

[82] a) K. Matsuda, M. Irie, *J. Am. Chem. Soc.* **2000**, *122*, 8309–8310; b) K. Matsuda, M. Irie, *J. Am. Chem. Soc.* **2000**, *122*, 7195–7201.

[83] S. Nakatsuji, H. Anzai, *J. Mater. Chem.* **1997**, *7*, 2161–2174.

[84] Besides the questionable chemical feasibility (including stability) of directly appending ethynyl to dangling SCs, the use of ethynyl as connectors has also been ruled out for methodological reasons[22] and because it often behaves as a poor spin coupler; see for instance: a) Y. Miura, T. Issiki, Y. Ushitani, Y. Teki, K. Itoh, *J. Mater. Chem.* **1996**, *6*, 1745–1750; b) Y. Miura, M. Matsumoto, Y. Ushitani, Y. Teki, T. Takui, K. Itoh, *Macromolecules* **1993**, *26*, 6673–6675; c) H. Nishide, T. Maeda, K. Oyaizu, E. Tsuchida, *J. Org. Chem.* **1999**, *64*, 7129–7134.

[85] For *enhanced isc*, see also: E. A. Weiss, E. T. Chernick, M. R. Wasielewski, *J. Am. Chem. Soc.* **2004**, *126*, 2326–2327.

 © 2008 Wiley-VCH Verlag GmbH & Co. KGaA, Weinheim

[86] For the 2-pyrimidine, $\Delta E(T_1-S_0)=3.22$ eV.
[87] Unfortunately, also, An-based "extended TTF" showing advantageous saddle-shaped distortion in the ground state cannot be used as a spin coupler. Indeed, the silole groups of the TTF moiety are more easily oxidized (giving axially distorted conformation) than tetrazone, which is the precursor of OV radical; see M′H. Chahma, X. S. Wang, A. van der Est, M. Pilkington, *J. Org. Chem.* **2006**, *71*, 2750–2755.
[88] Slight discrepancies between the data of the graphs and the values reported in the tables have to be ascribed to the fact that both the structures and the *J* values were computed using the $\text{Pople}_{\text{mix}}$ basis (see Computational Methods).
[89] a) L. Salem, *Acc. Chem. Res.* **1979**, *12*, 87–92; b) W. Schuddeboom, S. A. Jonker, J. M. Warman, M. P. De Haas, M. J. W. Vermeulen, W. F. Jager, B. De Lange, B. L. Feringa, R. W. Fessenden, *J. Am. Chem. Soc.* **1993**, *115*, 3286–3290; c) A. Viel, R. P. Krawczyk, U. Manthe, W. Domcke, *Angew. Chem.* **2003**, *115*, 3556–3559; *Angew. Chem. Int. Ed.* **2003**, *42*, 3434–3436.
[90] J. V. Lockard, J. I. Zink, Y. Luo, M. N. Weaver, A. E. Konradsson, J. W. Fowble, S. F. Nelsen, *J. Am. Chem. Soc.* **2006**, *128*, 16524–16531.
[91] J. M. Giaimo, A. V. Gusev, M. R. Wasielewski, *J. Am. Chem. Soc.* **2002**, *124*, 8530–8531.
[92] Note that the photoinduced symmetry breaking of the molecule has been shown to be assisted by its surrounding medium (solvent), see: a) T. Takaya, S. Saha, H. Hamaguchi, M. Sarkar, A. Samanta, K. Iwata, *J. Phys. Chem. A* **2006**, *110*, 4291–4295; b) F. C. Grozema, M. Swart, R. W. J. Zijlstra, J. J. Piet, L. D. A. Siebbeles, P. Th. van Duijnen, *J. Am. Chem. Soc.* **2005**, *127*, 11019–11028; and also ref. [91].
[93] The actual system should include surrounding molecules by which symmetry breaking is likely to be initiated.
[94] P. L. Luisi, *Found. Chem.* **2002**, *4*, 183–200.
[95] a) G. M. Whitesides, R. F. Ismagilov, *Science* **1999**, *284*, 89–92; b) I. R. Epstein, K. Showalter, *J. Phys. Chem.* **1996**, *100*, 13132–13147.
[96] a) R. F. Ludlow, S. Otto, *Chem. Soc. Rev.* **2008**, *37*, 101–108; b) P. T. Corbett, J. K. M. Sanders, S. Otto, *Angew. Chem.* **2007**, *119*, 9014–9017; *Angew. Chem. Int. Ed.* **2007**, *46*, 8858–8861.
[97] M. Ruben, U. Ziener, J.-M. Lehn, V. Ksenofontov, P. Gütlich, G. B. M. Vaughan, *Chem. Eur. J.* **2005**, *11*, 94–100.
[98] There are various approaches to emergent behaviors in chemistry, which do not necessarily entail close coupling of electronic nature at the intramolecular level. Opting for an intramolecular medium is here imposed by both the nature of the systems under consideration (PMDs) and the nature of the perturbing input (light). See for instance refs. [95–97]. For self-assembled nanostructures eliciting emergent behavior, see ref. [1d] and a) A. Müller, H. Reuter, S. Dillinger, *Angew. Chem.* **1995**, *107*, 2505–2539; *Angew. Chem. Int. Ed. Engl.* **1995**, *34*, 2328–2361; b) G. M. Whitesides, B. Grzybowski, *Science* **2002**, *295*, 2418–2421. See also: A. Lemarchand, L. Jullien, *J. Phys. Chem. A* **2004**, *108*, 11782–11791.
[99] M. R. Wasielewski, *Chem. Rev.* **1992**, *92*, 435–461, and references therein.
[100] In the illustrative case of bianthryl, a supersonic jet experiment provided evidence that interaction of this symmetric bipartite molecule with a single dissymmetric solvent molecule (e.g., acetonitrile) is sufficient to produce the photoinduced symmetry breaking process; see: K. Tanaka, K. Honma, *J. Phys. Chem. A* **2002**, *106*, 1926–1932.
[101] E. T. Chernick, Q. Mi, R. F. Kelley, E. A. Weiss, B. A. Jones, T. A. Marks, M. A. Ratner, M. R. Wasielewski, *J. Am. Chem. Soc.* **2006**, *128*, 4356–4364.
[102] M. J. Marsella, R. J. Reid, S. Estassi, L.-S. Wang, *J. Am. Chem. Soc.* **2002**, *124*, 12507–12510; S. Estassi, L.-S. Wang, *J. Am. Chem. Soc.* **2002**, *124*, 12507–12510.
[103] H. Güsten, M. Mintas, L. Klasinc, *J. Am. Chem. Soc.* **1980**, *102*, 7936–7937.
[104] The most promising PMMDs are to be experimentally investigated; work in progress.
[105] A. Rajca, *Chem. Rev.* **1994**, *94*, 871–893.
[106] S. Franzen, D. A. Shultz, *J. Phys. Chem. A* **2003**, *107*, 4292–4299, and references therein.
[107] O. Sato, J. Tao, Y.-Z. Zhang, *Angew. Chem.* **2007**, *119*, 2200–2236; *Angew. Chem. Int. Ed.* **2007**, *46*, 2152–2187, and references therein.

Received: July 10, 2008
Published online: November 14, 2008

 © 2008 Wiley-VCH Verlag GmbH & Co. KGaA, Weinheim